

# POLITECNICO DI TORINO

## Corso di Laurea Magistrale in Petroleum and Mining Engineering

Tesi di Laurea Magistrale

### Optimization of an LNG Storage Tank for the Minimization of the BOG for Three Different Liquid Filling Levels



**Relatore /i**  
prof. Nome e Cognome

**Candidato/i**  
Nome e Cognome

*firma del relatore*

*firma del candidato*

.....Laura Savoldi.....

.....Michel Obeid.....

## **Acknowledgment**

This study would not have been possible without the support and encouragement of Professor Laura Savoldi to whom I wish to express my deepest gratitude for her inspiring guidance, valuable discussion and for giving me the opportunity to do this thesis in the prestigious Politecnico di Torino. I owe a sincere thanks to my co-advisor Yifeng Zhang, Associate Professor at DTU, Technical University of Denmark for his constant support and feedback.

I would like to express my deep gratitude to my parents and my brother, if it was not for their unconditional support and help from the very beginning till the completion of this work I would not have been able to finish this project.

Last but not least, I would like to thank my friends in Italy and abroad who did not hesitate to help me whenever I needed them.

Finally, I would like to thank the department of Petroleum and Mining Engineering and the University of Politecnico di Torino for teaching and giving me a baggage of skills to kick start my career.

## LIST OF ABBREVIATIONS

NGV	Natural Gas Vehicles
LNG	Liquefied Natural Gas
NG	Natural Gas
IEA	International Energy Agency
FIP	Factory Instrument Protocol
ETAG	European Technical Approval Guidelines
BOG	Boil Off Gas
BOR	Boil Off Ratio
CFD	Computational Flow Dynamics
MAWP	Maximum Allowable Working Pressure
MTPA	Million Tons per Annum
NIST	National Institute of Standards and Technology
STP	Standard Conditions for Temperature and Pressure
PR-EoS	Peng Robinson Equation of State
LFL	Liquid Filling Level
CF	Carbon Footprint

## Abstract

The thermal performance of a 260000  $m^3$  LNG storage tank was studied for three different liquid filling levels. Thermodynamic equilibrium and non-equilibrium approaches were used to estimate BOG while incorporating a thermal resistance-capacitance network. After setting the tank parameters and initial fluid properties, convection and conduction heat transfers were calculated for the different parts of the tank as well as the vapor and liquid phases. It was possible then to compute the BOG and BOR of the three LFL of the tank. Our results indicate that the total heat leak variation disregards the liquid level of the tank, yet the BOG generated which is linked to the heat leak to the liquid phase of the tank increases with the decreasing filling level. For the 80% and 50% liquid filling levels the BOR was found to be 0.012 and 0.03wt%/day, respectively while for the 10% LFL a larger value equal to 0.152 was found which barely exceeds the threshold set in operating conditions that need to be furtherly treated. These results imply that vapor to liquid heat transfer has a major role in proper BOG calculation knowing that the heat ingress to the liquid phase is directly linked to this generation. Furthermore, with the data provided, the manufacturing carbon footprint of this tank was calculated and found to be  $88.5 \times 10^3$  carbon in tons CO<sub>2</sub>-eq.

## Table of Contents

Acknowledgment .....	2
LIST OF ABBREVIATIONS.....	3
Abstract.....	4
LIST OF TABLES.....	7
LIST OF FIGURES .....	8
Background.....	9
Chapter 1: Introduction.....	11
1.1 Fuel Importance.....	11
1.2 Transportation Fuel .....	11
1.3 LNG Importance .....	12
1.4 LNG Terminal.....	15
1.5 LNG Tanks.....	16
1.6 Literature Review on BOG studies and Thesis Aim.....	19
Chapter 2: Physical Phenomena Occurring in a LNG Tank.....	21
2.1 BOG Generation.....	21
2.2 BOG Importance.....	22
2.3 BOR.....	24
2.4 Weathering.....	24
2.5 Liquid Filling Level Effect.....	28
2.6 Thermophysical Properties of Liquid Phase.....	29
2.7 Thermophysical Properties of Vapor Phase .....	30
Chapter 3: Model Development.....	32
3.1 Methodologies and Assumptions .....	32
3.2 Mass Balance Analogy.....	33
3.3 Energy Balance Analogy.....	35
3.4 Heat Transfer through Tank Shell.....	37
3.4.1 Bottom.....	37
3.4.2 Roof.....	38
3.4.3 Walls.....	38
3.5 Heat transfer rate at the liquid vapor interface.....	41
Chapter 4: Case Study.....	43

4.1	Tank Parameters and Materials .....	44
4.2	Numerical Development .....	47
4.3	Model Results.....	53
4.3.1	Tank filled with 80% LNG .....	53
4.3.2	Tank filled with 50% LNG .....	54
4.3.3	Tank filled with 10% LNG .....	55
4.4	Discussion .....	56
4.5	Comparison with previous results .....	58
Chapter 5: Environmental aspect of technology presented.....		60
5.1	Future improvements and limitations .....	62
Chapter 6: Conclusion.....		63
<b>Appendices</b> .....		65
References.....		69

## LIST OF TABLES

Table 1: Constant coefficients in Eq. to calculate the thermophysical properties of LNG. ....	30
Table 2: LNG storage tank modeling parameters .....	44
Table 3: Density and Specific heat values for the insulating materials .....	45
Table 4: Variables in the calculation of the convection transfer coefficients on the wall. ....	48
Table 5: Summary of the different initial temperatures .....	48
Table 6: Height of liquid and vapor phases for the three different liquid filling levels .....	50
Table 7: Rayleigh number and heat transfer coefficients ( $W/m^2.K$ ) for the different parts of the wall.....	50
Table 8: Inner and outer wall temperatures in contact with the liquid and vapor phases for the three different liquid filling levels .....	51
Table 9: Heat Leakage, BOG and BOR for the three LFL .....	52
Table 10: Parameters used for the manufacturing CF calculation .....	61

## LIST OF FIGURES

Figure 1 Phase Diagram of Natural Gas[10].....	13
Figure 2 LNG supply chain scheme [14].....	14
Figure 3: Process flow of a typical LNG receiving and regasification terminal [16].....	15
Figure 4: Earth-sheltered LNG Underground Tank [18].....	16
Figure 5: In-ground LNG Storage Tank [18].....	16
Figure 6: Double Shell Horizontal Tank (Perlite Insulated) [14].....	17
Figure 7: Double shell vertical tank (Perlite Insulated)[14].....	17
Figure 8: Schematic of LNG storage tank during heat ingress [33].....	22
Figure 9: Schematic of the heat exchange between the surroundings, LNG and vapor [41].....	26
Figure 10: Variation of the heat ingress into the vapor $Q_{v,in}$ and the vapor/liquid heat transfer rate $Q_{vl}$ predicted by both the current model (c) and Migliore et. Al (M) as a function of time [37].....	27
Figure 11: Variation of the vapor to liquid heat transfer variation as a function of time [37].....	28
Figure 12 Heat Transfer from the Environment to Liquid and Vapor Phases through Tank Wall	39
Figure 13 Heat transfer from environment to liquid and vapor phases through tank wall.....	39
Figure 14: Flow chart for solving equations for the thermodynamic equilibrium modeling.....	43
Figure 15: LNG vertical storage tank [51].....	45
Figure 16: Total heat leak to the tank.....	55
Figure 17: BOG from liquid heat leak.....	56
Figure 18: BOR from heat leakage to tank.....	56
Figure 19: Static vs Dynamic BOR in LNG tank.....	57
Figure 20: BOR comparison chart between previous and current study.....	59
Figure 21: Tank Life Cycle [56].....	60

## Background

Energy supply is and will always be the biggest concern threatening the modern world. The increasing demand of resources to meet the needs of more than 7 billion people drives researchers to understand better the humans' consumption of the Earth's ecosystem [1]. To face this challenge, humans are constantly searching for energy sources and creating storage facilities to provide for the masses. Traditional energy sources used in the past years until now consist of the hydrocarbon family such as oil, natural gas, and coal. While the planet's survival depends on this increasing production and consumption cycle, a shortage of such resources has to take place in the near future but will not be due to availability problems. To be more precise, this shortage will challenge oil and gas producers significantly in order to address climate change and the rise in temperature envisioned by the Paris agreement. In a study developed by Neal Anderson, president, and CEO of Wood Mackenzie the world's leading energy and consulting firm, in 2040, hydrocarbon will still provide 80% of the world's energy use, mainly coal, natural gas and crude oil [2]. Efforts to reduce such projection are being pursued with sustainability and energy efficiency is seen as the ultimate goals; unfortunately, green technologies are still a bit behind when it comes to answering the masses demand due to their lower efficiency, insufficient technical development and market handicap. Looking forward to achieving a complete sustainable eco-friendly future, for the time being, acting fast and handling energy and environmental policies have to be coupled together to achieve a vital energy transition in order to ensure such a future [3]. Knowing that this energy shift is promising, it is not wrong to take a look at what is present and try to improve the oil and gas industry as much as possible aiming towards a zero-carbon emission technologies. A solid example that highlights a big entity in favor of this shift, is the Paris Agreement characterized as a legally conclusive treaty on climate change adopted by 196 parties in late 2015 and entered into force on

November 2016 [4]. The Paris Agreement defines a global goal on adaptation to the climate change while preventing a global warming above 2°C with constant effort to hold the global temperature rise below 1.5°C. By implying a transparency framework, the Paris Agreement parties would be sharing information about climate change impacts and acclimation as well as actions that should be taken to reduce greenhouse gas emissions; therefore, a collective effort towards mitigation sets a firm path towards achieving short and long term goals. Whether in the production, refining or storage and transportation sector, improvements can be and must be made in parallel with the alternative energy campaign.

## **Chapter 1: Introduction**

### **1.1 Fuel Importance**

While earth's natural resources are not fully known or even fixed in any sense, beneath layers of rock and sediments lies the remains of plants and other organisms, decomposed over millennia into carbon-rich deposits known as fossil fuel. Fossil fuels include coal, oil shales, petroleum, bitumen, tar sands, heavy oils, and natural gas. Each of these fossil fuels can be burned in presence of oxygen in order to provide heat that can be either employed directly in households (furnaces, room heater), or applied to produce steam for generators to further supply electricity. These fuels are being consumed at an increasing rate counting from the industrial revolution in Great Britain in the late 1700s up until the present moment where they consist of more than 80% of the world's energy supply [5]. Being one of the most widely-used energy sources, fuel burning has many applications such as providing electricity for houses and facilities as well as powering engines, vehicles, airplanes, and ships.

### **1.2 Transportation Fuel**

All energy sources derived from petroleum, biomass, and synthetic fuel that power any mean of transport are considered transportation fuel. Gasoline and diesel account for the highest share of the total transportation fuel consumed by road transport. On the other hand, the aviation industry focuses on aviation turbine fuel while the railway industry consumes diesel or electricity. These fuels are nothing but the end products of crude oil refining and account for almost 90% of the transportation fuel worldwide [6]. This spiking dependency on crude oil is reflected negatively when it comes to high emission levels and greenhouse gas emissions into the atmosphere, the main stimulants for climate change. Government and organizations around the world started developing

and promoting the use of cleaner eco-friendly fuels. Among those fuels, natural gas stands on the verge between traditional fuel and green energy, especially that it is considered the cleanest burning fossil fuel due to its chemical composition, emitting half as much CO<sub>2</sub> as coal to produce the same amount of energy[7]. The use of natural gas as an alternative fuel in the transportation sector goes way back to the 1930's when it was used to fuel vehicles. Recently with technological advancement, proliferation of natural gas cars and buses has become available which is contributing to cleaner vehicles and transportation facilities in the world [8]. In fact, natural gas vehicles (NGVs) have many pros such as improving air quality and reducing noise pollution in urban regions, creating a divergence from consuming oil into exporting it but also improving energy security and reduce spending on public transportation. Being considered as a clean and low emission energy source, natural gas or even liquefied natural gas (LNG) production is becoming the new hotspot in the oil and gas market, and the results are being observed in the transportation industry where companies and governments are putting more investments and attention to NG/LNG [9].

### **1.3 LNG Importance**

Liquefied natural gas (LNG) is the liquid state of natural gas after dropping its temperature to -161°C. The phase diagram of a normal natural gas composition can be seen in Figure 1

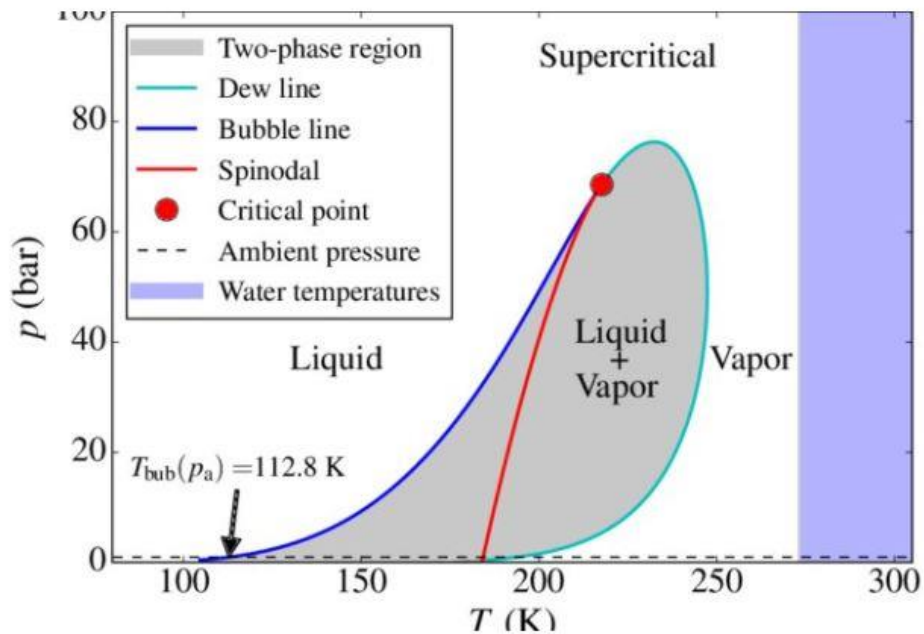


Figure 1 Phase Diagram of Natural Gas[10]

In the liquid state the volume of NG is 600 times smaller than the one in its gaseous state, which made this liquefaction process a great technology that overstepped the transportation limitations and allowed the use of natural gas in the transportation sector [11]. LNG has become a solution for land and marine transportation as well as one of the main sources for petrochemicals and power generation . Apart from having a reduced volume when in liquid state, it has a more stable structure compared to pipeline gas which makes its delivery more practical. Moreover, LNG owns higher and safer quality gas, purer by having a higher methane content and safer by the fact that any vapor released from LNG does not imply an explosion risk in unconfined spaces, even in the case of a gas spill. Another benefit of LNG is that it is very flexible by the means of trading where cargoes of LNG can be easily shipped which results in cheaper transportation compared to traditional gas [12]. The market share of LNG continuously increasing in the global fuel trade. In fact, GasLog – an international LNG owner and operator – stated that the total LNG demand

increased by 9% between 2017 and 2018 [13]. Having mentioned that LNG is one of the best ways to ensure safe, economic and eco-friendly natural gas transportation, a major drawback of LNG is its projects including LNG terminals and storage facilities.

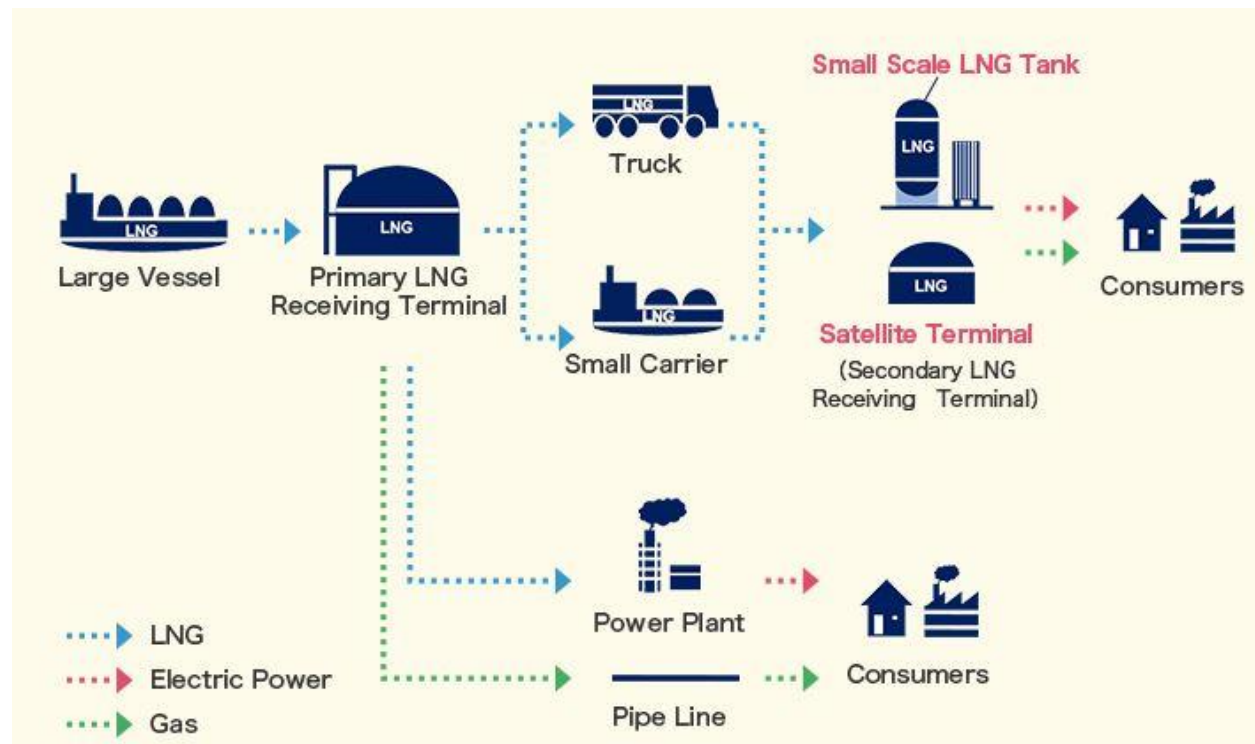


Figure 2 LNG supply chain scheme [14]

## 1.4 LNG Terminal

An LNG terminal is a facility where loading/unloading of LNG cargo to and from ship tankers takes place Figure 3. Once the ships reach the quay of the terminal, the LNG is received at its very low temperature ( $-162^{\circ}\text{C}$ ) while being transferred to storage tanks using three arms (special pipes). These arms are insulated to prevent heat exchange from the air thus minimizing the vaporization of LNG and are connected to pipelines that end up in the storage tanks. From these insulated tanks, LNG is then drawn out from the tanks, pressurized, and regasified using heat exchangers converting in this way the LNG from liquid back to its gaseous form. This process requires a high amount of heat in order to increase the LNG's temperature from  $-162^{\circ}\text{C}$  to  $0$  or  $10^{\circ}\text{C}$  and introduce it back into pipelines. At this point, propane might be added in order to enrich the gas or nitrogen in order to dilute it. Finally, before sending out the gas into the transmission grid, this regasified natural gas is metered and dosed using an odorizing agent [15].

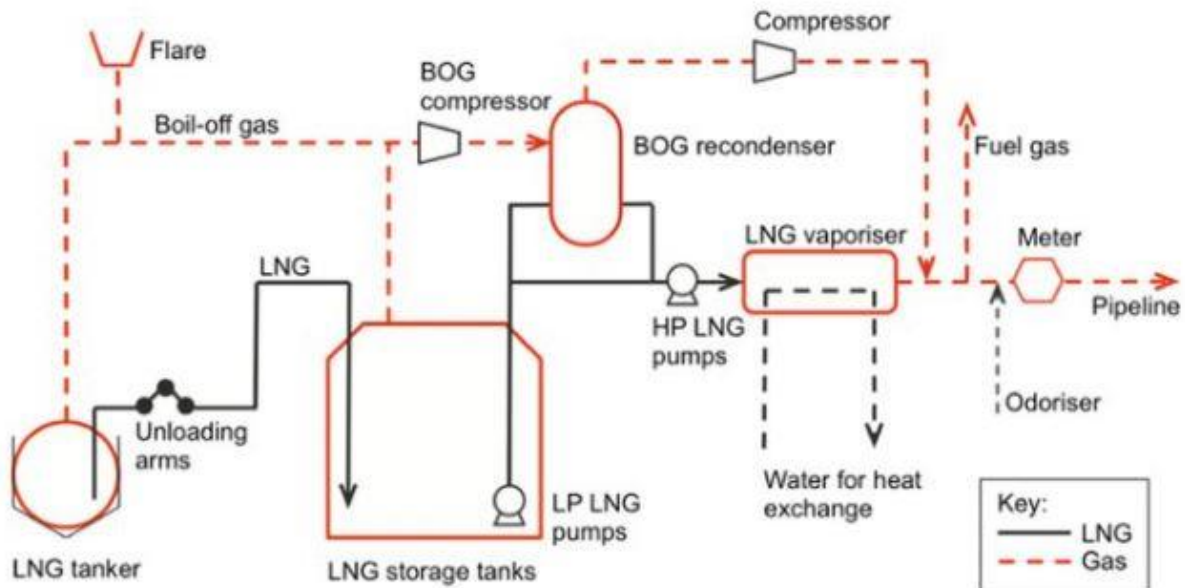


Figure 3: Process flow of a typical LNG receiving and regasification terminal [16]

## 1.5 LNG Tanks

This sprouting in LNG use over the recent years required a simultaneous development and design of LNG storage tanks essential for receiving and safely storing the liquefied gas. These particularly engineered massive tanks are designed using a double-walled construction approach with insulating materials that can sustain very low temperatures ( $162^{\circ}\text{C}$ ). Other than maintaining the temperature constant, the storage structure has to be rigorous and robust taking into account their ability to sustain stress, strain, or any unexpected deformation. These tanks are usually constructed and installed under firmly controlled conditions and regulations with hardware requiring official certifications. In a receiving terminal, tanks could be installed both underground – here 2 types can be distinguished: Earth-sheltered LNG underground tank where the tank is completely buried with its roof Figure 4 with a huge storage capacity and In-ground LNG storage tank Figure 5 where the storage part is buried while the roof remains on the surface [18]– and above ground being either horizontal Figure 6 or vertical Figure 7 tanks [14].



*Figure 4: Earth-sheltered LNG Underground Tank [18]*



*Figure 5: In-ground LNG Storage Tank [18]*

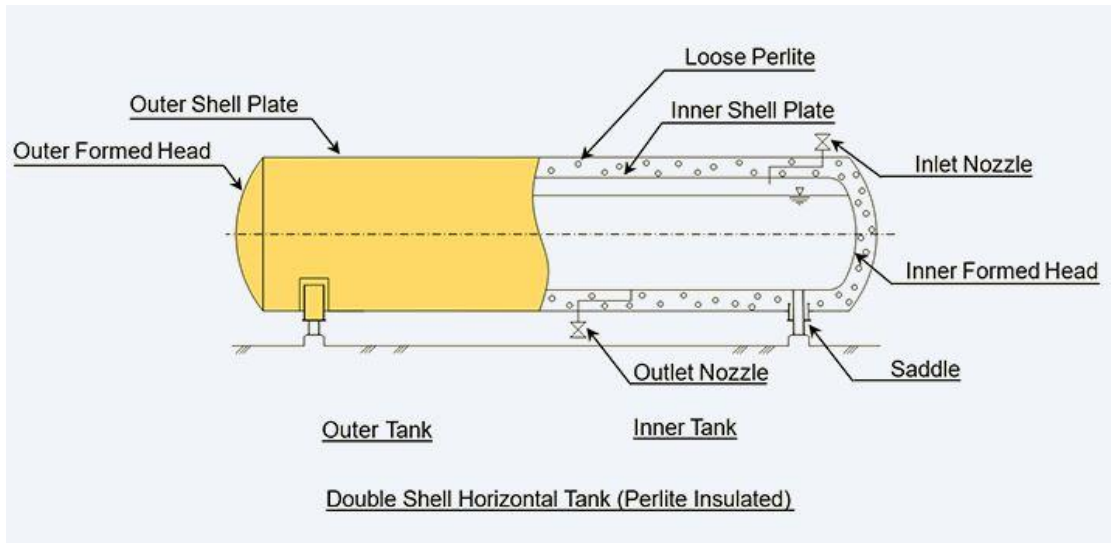


Figure 6: Double Shell Horizontal Tank (Pelite Insulated) [14]

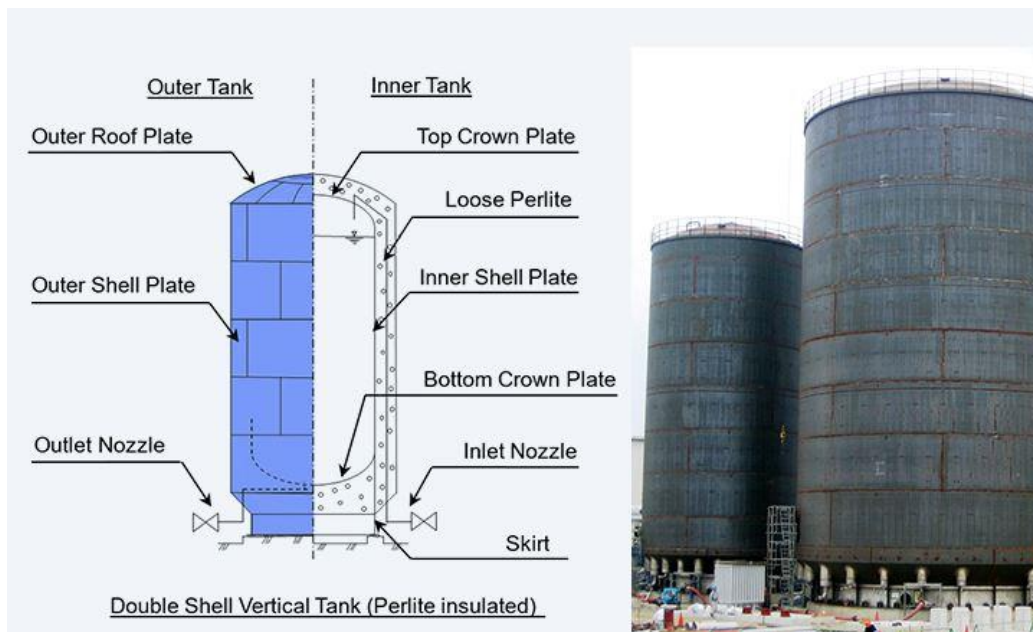


Figure 7: Double shell vertical tank (Pelite Insulated)[14]

Vertically designed tanks have typical dimensions of the order of 50m in height and 80 to 90m in diameter, and the principal contractor normally determines the specific design requirements of the

pre-stressed concrete that consists the outer shell or containment of the tank [18]. No official standard design has been implemented for such tanks however testing is required to be carried out, according to the *FIP* SR 88/2 guidelines[19], on pre-stressing steel, tendon assembly and load transfer (at both room and cryogenic temperatures). Subsequently, more recent guidelines –ETAG 013 – were published[19] and require the following tests to be carried out: Stressing the tendon to almost 80% of its proper tensile strength, decreasing the temperature to -196°C and loading the tendon to failure. These tests are a huge part of the quality control that is essential for the successful performance of the tank. While the exterior part of the storage tank is mainly concrete walls, the inner part is made of a specific nickel/steel alloy along with several insulation layers mainly glass wool and expander perlite to host the cold LNG. With a capacity of 18.2 million cubic meters, Japan holds the first position with the world's largest LNG storage tank, followed by South Korea and China with LNG tank storage capacities of 12.4M and 10.7M cubic meters respectively [19].

While LNG storage tanks are designed to be of different sizes, several ways of containment are employed (single, double, full and membrane)[20]. The single containment type is made of an inner 9% nickel-steel cylindrical container with outer insulation (i.e., perlite) surrounding it; on the other hand, in double and full containment types, inner and outer tanks host the LNG [21]. Full containment tanks are known for being the most advanced types that are currently employed in the industry, having an inner lining made of 9% nickel-steel alloy that is ductile at very low temperatures. To limit heat leakage, the internal nickel-steel fixing is cushioned with various layers of insulating fabrics glass wool, sand, plywood and expanded perlite[21].

## 1.6 Literature Review on BOG studies and Thesis Aim

Even though LNG is stored in highly insulated storage tanks, LNG vaporization denoted as boil-off gas (BOG) is commonly faced in tanks due to the parasitic load from the environment. BOG undermines the compression work involved in natural gas (NG) liquefaction, and its minimization improves the economics of the LNG value chain. While BOG depends on the heat ingress, its assessment depends on the modelling and measuring capability while the tank design and operating conditions affect the difficulty of this accurate assessment. Numerous experimental studies aiming to accurately predict the BOG and BOR in storage tanks have been carried out over the years, however, the liquefied gas was inert such as nitrogen or helium due to the risk of explosion [22]. On the other hand, in real industrial practices this gas is active such as natural gas or hydrogen while being hard to handle experimentally. In addition, experimental studies are based on lab-scale approaches that cannot reflect the genuine state of large static pressure of industrial-scale tanks. This inconsistency in static pressure causes the boiling temperature to be also discrepant with actual practices. Furthermore, these studies based on scaling down and up, will of course affect the surface area to volume ratios which will directly have an influence on the heat transfer characteristics and internal flow dynamics inside the tank [22]. Knowing that such errors are unavoidable, investigating the BOG and BOR experimentally seems a bit impractical. For this reason, studying the BOG and BOR more accurately is preferred to be done theoretically using conventional numerical analysis and implying them into computational fluid dynamics (CFD) simulations that enable graphic visualization of fluid motion. CFD methods were applied to solve multi-phase problems in multiple areas such as chemical processes, nuclear energy, automotive, and aerospace industries. Hassanvan et al. developed the CFD simulation of the vaporization of gasoline in a car tank during splash loading with a solid comparison between numerical results and

theoretical values [23]. Lee et al. and Fu et al. were the ones that simulated the vaporization of cryogenic liquid using the phase change model. Lee et al. [24] simulated the LNG leakage from a membrane tank while applying a diffusion model to monitor the phase change of the LNG through the porous membrane. Then, after developing the phase change model using ANSYS Fluent, the codes were improved through several researches. Fu et al. [25] were able to link the vaporization effect to the internal tank pressure by carrying CFD simulation of the phase change of liquid hydrogen in spacecraft fuel tank, this change due to gravity and surface tension. Zakaria et al. [26] were able to find the BOG of a full-scale ship tank using ANSYS Fluent however the study was missing the geometry description and the numerical analysis. Ahammad et al. developed numerical research on the vaporization frequency of LNG and nitrogen on a film boiling inside a storage tank and visualized the physics for the analysis [27]. Saleem et al. [28] carried out a CFD simulation on the BOG inside a full-scale LNG storage tank and reported the effects of the numerical data of the phase change on the results. Almost all of the mentioned studies carried out the effect of input parameters of the phase change and boundary conditions modifications.

This project aims to estimate the BOG generation and the BOR in a  $2.6 \times 10^5 m^3$  tank for different LNG filling levels (80%, 50%, and 10%). In the present study, a thermodynamic equilibrium and non-equilibrium approach based on the resistance-capacitance link will be used to investigate the thermal performance of this LNG storage tank. Also a brief carbon footprint of this technology is carried out.

## Chapter 2: Physical Phenomena Occurring in a LNG Tank

### 2.1 BOG Generation

As previously mentioned LNG is stored in storage tanks as a cryogenic liquid or in other words extremely cold liquid. Just like any other liquid, when the boiling temperature is reached evaporation is an expected phenomenon that might take place. Liquefied natural gas evaporates at temperatures exceeding its boiling point and generates Boil Off Gas or BOG [29]. This boil off is caused by heat ingress into the liquid whether during storage, transportation, loading, and unloading operations. BOG quantity is based also on the design of storage tanks as well as the operating conditions [29]. BOG is the main reason behind the overall tank pressure increase. In fact, while the 2 phase mixture is at rest at a constant volume, heat ingress will cause a part of the liquefied natural gas to evaporate and return to its gaseous state having a larger volume and leading to the pressure increase in the tank. In order to avoid over-pressurization, and maintain the pressure below the maximum allowable working pressure (MAWP) the BOG generated is continuously removed by BOG compressors. However, the BOG released gradually decreases the methane concentration which can affect the combustion quality of LNG. For this reason, studying this vaporization and estimating an accurate BOG amount will for sure be a basis for developing potential uses of this BOG.

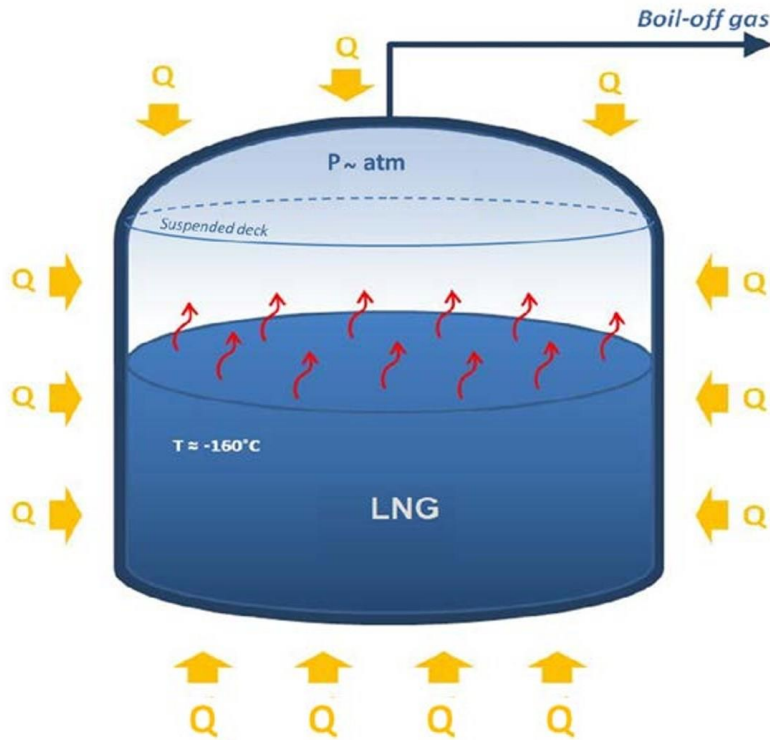


Figure 8: Schematic of LNG storage tank during heat ingress [33]

## 2.2 BOG Importance

The LNG industry tend to diminish this BOG generation by seeking optimal design of tanks and pipes with the finest insulating materials. However, controlling the environment is not in the hands of scientists or engineers, thus vaporization cannot be avoided [29]. During boil off, the first components to evaporate are the most volatile (methane, nitrogen), changing the composition of the liquefied natural gas and its quality with time. This phenomenon is denoted as ageing or weathering and is critical in LNG trading since this fuel's price in the market is affected by its energy content. In fact, LNG producers identify the quality of their LNG based on the field gas composition and more specifically market demand [29]. Therefore, knowing the amount of the

BOG generated or even the Boil-Off Rate (BOR) in a storage tank gives more or less an inclusive image about the LNG quality. The BOG rate (kg/s) can be defined as

(1)

$$BOG \left( \frac{kg}{h} \right) = \frac{Q \left( \frac{kJ}{s} \right)}{\lambda \left( \frac{kJ}{kg} \right)} * 3600$$

Where  $Q_{liquid}$  is the total heat leakage (kJ/s) to the liquid through the walls and the heat indirectly received from the vapor phase [28] and  $\lambda$  the latent heat of vaporization of LNG (kJ/kg). Although heat is also exchanged at the vapor liquid interface, its contribution is negligible compared to the heat ingress to the liquid through the tank walls

While the global LNG regasification capacity increased to 825 MTPA (million tons per annum) as of February 2019, and around 130 MTPA are currently under development [30], it is the upmost necessary to accurately estimate BOG generations under different operating conditions, followed by placing cost-effective procedures for the recycling and application of this gas [31]. To be more precise, in the LNG supply chain the boil off gas generated can be considered as a fuel thus directly used for power generation or heat, re-liquefied back into the storage tank or burned in a gasification unit. While this last alternative poses environmental problems, it is absolutely preferable to use this boil off gas to power an electric generator or be re-liquefied. The power provided using this BOG can be estimated using  $P = \left( \frac{m\rho}{M} \right) * \Delta H_c * \varepsilon_w$  where  $\Delta H_c$  is the heat of combustion of CH<sub>4</sub> and  $\varepsilon_w$  is the methane electricity conversion efficiency [32]. In some cases, given that the BOG

flow rate is considered an indicator instead of tracking the pressurization that requires a long time to be accurately detected [34].

### 2.3 BOR

The Boil-off rate (BOR), LNG vaporization of the total LNG mass per day [wt%] is defined as:

(2)

$$BOR = \frac{BOG_{liq} \times 24}{Total\_LNG\_mass} * 100$$

BOR is defined as the quantity of liquid being evaporated from its storage container due to heat ingress and it is expressed in % of the total liquid volume per unit time. Typically BOR values are equal or less than 0.15%/day, the lower the percentage the better [35].

### 2.4 Weathering

Before starting any mathematical development, it is important to state that the liquid is evaporating. It is therefore essential to know the behavior of such evaporation.

In fact, evaporation causes LNG to become denser thus changing its composition. This change in composition will influence the thermophysical properties and its heating value essential for export to grid stability [36]. This progressive alteration of thermophysical properties of stored LNG through vaporization is summarized by ‘weathering’.

Weathering estimation of stored LNG is of a major importance to the industry especially in the operation of regasification facilities. Increase in LNG storage time is being induced by sudden variation in gas prices and seasonality, for this reason predicting accurately the weathering taking place is essential in evaluating the accordance between the stored LNG and the supplied gas system

to final consumers. Also, when the LNG undergoes a significant weathering in the tank it will become richer in heavy components; as a consequence, its density and boiling temperature will increase which might call for action to introduce a new LNG batch that is lighter and cooler. This process comes with a number of undesirable events such as stratification, sudden vapor liberation and roll-over which might put at risk the business as usual [33].

Initial weathering models based on the ingress of heat started in the 1960s assuming an under steady state in order to find the wall temperature profile and to get an estimation of the maximum BOR [37]. Thirty years later, the first transient model of weathering was developed (the Shah and Aarts model) which revived the LNG storage modelling [38]. In fact, this model was included in several research tending to improve the thermodynamic model. At the same time, Chen et al. focused on pure methane evaporation in storage tanks to follow the pressure and temperature trends[32] while Adom et al. worked on a model that relates the operating pressure on boil off gas rates [39]. It was Pellegrini et al. [40] that simplified the vapor liquid phase calculations by removing the constant thermophysical properties assumption which helped Migliore and co-workers [33] to develop a weathering model focused on pure heat transfer and phase equilibria sub-models taking out the constant heat ingress assumption. Thermal equilibrium between liquid and vapor natural gas was the common assumption in all of the above mentioned studies. Recently, weathering models got rid of this assumption between liquid and vapor phases after industrial proof of vapor superheating. This means that the vapor acts as an additional heating source knowing that it has a higher temperature than the liquid after treating the heat ingress into the vapor section separately from the liquid one.

In order to better understand this mechanism, a closer look on **the vapor liquid heat transfer analysis** shows the following:

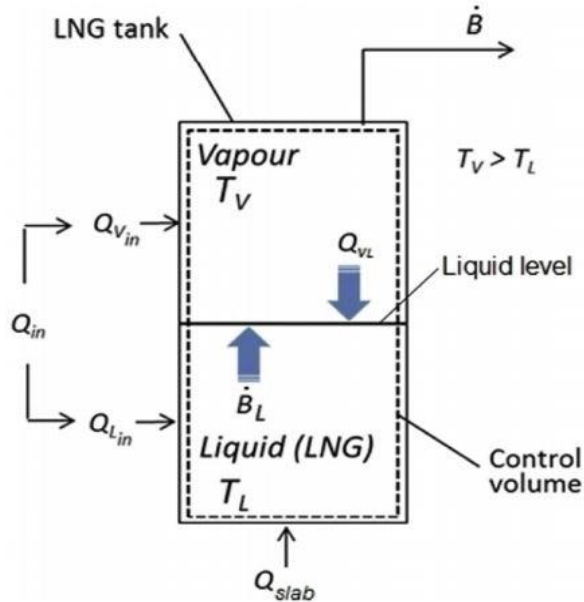


Figure 9: Schematic of the heat exchange between the surroundings, LNG and vapor [41]

As it is clear in Figure 9, the heat entering the tank is treated separately between the vapor and liquid phases. Heat entering the liquid phase  $Q_{Lin}$  will slowly increase its boiling temperature whether due to the change of LNG composition (richer in heavy components) or due to the increase in pressure. Also, heat entering the vapor phase  $Q_{vin}$  will increase its temperature. Therefore,  $T_{vap} \geq T_{liq}$  and the superheated vapor acts as an additional heating source for the liquid, leading to heat transfer from the vapor phase to the liquid phase,  $Q_{vl}$ . This vapor liquid heat transfer rate does not only depend on the temperature difference but also on the heat transfer mechanism in the vapor and the interface. First, Effendy et al. [42] studied the LNG storage procedure in a regasification terminal while considering the vapor heated by pure convection. It was Migliore et al. [41] that considered two limiting scenarios for the heat transfer within vapor, convection and

conduction after developing a non-equilibrium weathering model. As a result of their work, the vapor temperature witnesses an average increase of 8K per year induced by a conductive vapor to liquid heat transfer for a tank filled with LNG [41]. This goes in parallel with obvious industrial evidence on vapor superheating which goes beyond words to acknowledge that conduction is the dominant heat transfer mechanism in the vapor phase.

On another note, in a study developed by Felipe Huerta and Velisa Vesovic [37] that takes the previous model of Migliore et al. (who developed the non-equilibrium weathering model for an LNG storage tank), temperature profiles and heat transfer scenarios were monitored.

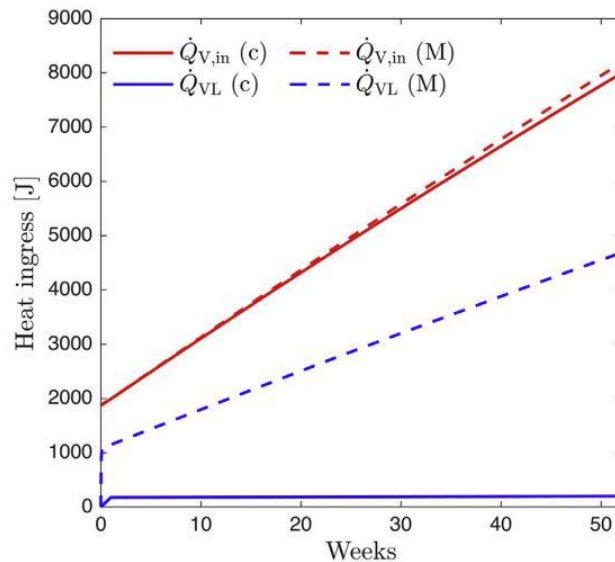


Figure 10: Variation of the heat ingress into the vapor  $\dot{Q}_{v,in}$  and the vapor/liquid heat transfer rate  $\dot{Q}_{vL}$  predicted by both the current model (c) and Migliore et. Al (M) as a function of time [37].

In Figure 10, the low  $\dot{Q}_{vL}$  trend predicted by the current model (Felipe and Velisa), match with the CFD model developed by Roh and Son [43] that shows that  $\dot{Q}_{vL}$  contributed to 0.01% of the heat ingress thus negligible, and the experimental observations of Lin et al. that confirm these

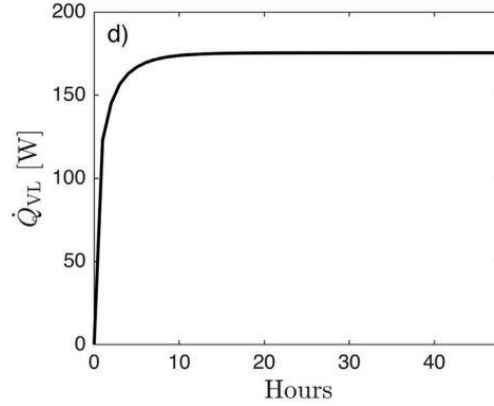


Figure 11: Variation of the vapor to liquid heat transfer variation as a function of time [37]

prediction models allow us to say that the almost constant  $Q_{vl}$  during evaporation suggests the presence an early transient period prior to a quasi-steady state

Figure 11 shows that at early times  $Q_{vl}$  increases rapidly as the temperature gradient at the interface increases. It then reaches a constant value once the quasi-steady state temperature profile is reached.

## 2.5 Liquid Filling Level Effect

While studying this evaporation, it is also important to notice the effect of the liquid filling levels on the heat transfer to the vapor, the liquid and between both at the interface.

Logically speaking, the heat ingress into the vapor ' $\dot{Q}_{v,wall}$ ' (W) [44] increases with decreasing liquid filling levels because the vapor area increases, in fact:

(3)

$$\dot{Q}_{v,wall} = U_v * A_{inner\ wall,v} * (T_{air} - T_v)$$

$U_v$ : Overall heat transfer coefficient ( $W/m^2K$ ) based on the external contact area.

$A_{inner\ wall,v}$ : Area of cylinder ( $m^2$ ) with the inner diameter of the tank and a height equivalent to the vapor phase.

Thus for a lower liquid filling level (50% or 10%) more vapor area is available for heat transfer compared to a higher liquid filling level (80%). Consequently, more heat transfer will induce a rise in temperature of the vapor which will cause a heat transfer from this vapor to the LNG via the vapor-liquid interface. So, the initial vapor to liquid heat transfer ' $Q_{vl}$ ' increases with decreasing liquid levels due to larger temperature gradients at the interface, however the variation is small compared to the decrease of ' $Q_l$ ' (when the area of liquid is smaller).

To sum up, the smaller the initial liquid filling, the higher the heat transfer to the vapor, from vapor to the liquid as well and therefore a higher BOG rate is expected.

## 2.6 Thermophysical Properties of Liquid Phase

The main thermo-physical properties of liquid natural gas are present as a function of LNG temperature  $T_l$ . These thermos-physical properties are the specific heat capacity  $C_{p,l}$ , the density  $\rho_l$ , the viscosity  $\mu_l$ , conductivity  $k_l$ , and thermal expansion coefficient  $\beta_l$ . These functions are fitted with the data provided by the National Institute of Standards and Technology (NIST) [45] following this equation:

$$f(T_l) = c_0 + c_1T_l + c_2T_l^2 + c_3T_l^3 + c_4T_l^4 + c_5T_l^5 + c_6T_l^6$$

(4)

The constant coefficients in this equation are given in Table 1 below:

Table 1: Constant coefficients in Eq. to calculate the thermophysical properties of LNG [45].

$f(T_l)$	Unit	$c_0$	$c_1$	$c_2$	$c_3$	$c_4$	$c_5$	$c_6$
$\rho_l$	$kg/m^3$	$-2.554 \times 10^4$	$1.199 \times 10^3$	$-22.792$	$0.228$	$-1.2785$	$3.779$	$-4.618$
						$\times 10^{-3}$	$\times 10^{-6}$	$\times 10^{-9}$
$C_{p,l}$	$J/kg.K$	$-5848$	$231.4$	$-1.965$	$0.0057$	$-$	$-$	$-$
$\mu_l$	$kg/m.s$	$0.0013$	$-2.231 \times 10^{-5}$	$1.332$	$-2.743$	$-$	$-$	$-$
				$\times 10^{-7}$	$\times 10^{-10}$			
$k_l$	$W/m.K$	$0.2109$	$1.546 \times 10^{-3}$	$-2.186$	$5.268$	$-$	$-$	$-$
				$\times 10^{-5}$	$\times 10^{-8}$			

As for the thermal expansion coefficient  $\beta_l$ , it is calculated by equation (5) using the thermophysical properties of methane at a reference temperature of  $T_l = -162^\circ\text{C} = 111.15\text{K}$  where  $\rho_l = 422.6 \text{ kg/m}^3$  [54]

(5)

$$\beta_l = -\frac{d\rho_l}{dT_l} \frac{1}{\rho_l}$$

## 2.7 Thermophysical Properties of Vapor Phase

Calculating the specific heat capacity, density and enthalpy of the vapor phase requires an adequate thermodynamic state model. In our study, the Peng-Robinson equation of state (PR-EoS) is applied knowing that it was originally developed to compute the thermodynamic properties of NG, then was widely used in the oil and gas industry due to its simplicity and mutability. The PR-EoS [45] is expressed as:

(6)

$$P = \frac{RT}{(v - b)} - \frac{a}{v^2 + 2bv - b^2}$$

Where,

(7)

$$a = 0.452724 \frac{R_u^2 T_c^2}{P_c} \left[ 1 + f_\omega \left( 1 - T_r^{\frac{1}{2}} \right) \right]^2$$

(8)

$$b = 0.0778 \frac{R_u T_c}{P_c}$$

(9)

$$f_\omega = 0.37464 + 1.54226\omega - 0.26992\omega^2$$

(10)

$$T_r = \frac{T}{T_c}$$

The parameters  $P_c$ ,  $T_c$  and  $\omega$  are the critical pressure and temperature, and the acentric factor which is a function of the saturated vapor pressure and the critical pressure, respectively. For methane [45]  $P_c = 4.599 \text{ MPa}$ ,  $T_c = 190.564 \text{ K}$ , and  $\omega = \frac{P_{sat}}{P_c} = \frac{116000}{4599000} = 0.025$ . While  $f_\omega$  is just a coefficient in the Peng Robinson equation (9),  $R_u$  or  $R$  is the universal gas constant equal to  $8.314 \text{ J/molK}$  and  $v = 0.024 \text{ m}^3/\text{mol}$  the molar volume at STP. In order to calculate the molar enthalpy (J/mol) of the vapor phase, residual enthalpy is used [33] :

(11)

$$h - h^{ideal} = Pv - RT \int_{\infty}^v \left[ T \left( \frac{\partial P}{\partial T} \right)_v - P \right] dv$$

where,  $h^{ideal}$  is the ideal gas enthalpy given by,

(12)

$$h^{ideal} = h_{ref} + \int_{T_{ref}}^T C_p dT$$

Substituting the PR-EoS equation (9) into equation (11) one obtains,

(13)

$$h - h^{ideal} = Pv - RT - \frac{1}{2\sqrt{2}b} \left( a - T \frac{da}{dT} \right) \ln \left( \frac{v + (1 + \sqrt{2})b}{v + (1 - \sqrt{2})b} \right)$$

Therefore, one can compute the molar enthalpy at a certain temperature and density.

## Chapter 3: Model Development

### 3.1 Methodologies and Assumptions

A lot of models have been developed invoking the assumption that the stored cryogenic fuel is in a thermal equilibrium state. This means that the vapor and liquid temperatures are equal. In such models, input data requires the tank parameters and geometry, the initial temperature, pressure and liquid filling level while the output parameters are the tank pressure and temperature and liquid filling level as well as the wall temperature [44]. At the vapor liquid interface, the heat and mass transfer are calculated repeatedly at each time step until the temperature difference satisfies the convergence term  $|T_v - T_{sat}|$  and  $|T_l - T_{sat}| < (\epsilon = 10^{-3}K)$ .

In the non-equilibrium model, the two phases have different temperatures. While the input and output parameters are similar to the case of equilibrium modeling, the heat and mass transfer at the vapor liquid interface are solved once at each time step without equalizing  $T_l$  and  $T_v$ . A non-equilibrium model such as the one developed by Migliore et al. [41] justifies how the vapor acts as an additional heating source where  $T_v \geq T_l$ , leading to an additional heat transfer at the liquid-vapor interface  $Q_{vl}$ .

However, in the study developed by Wang et al. [44], where a thermodynamic non-equilibrium model was introduced to assess the thermal performance of an LNG storage tank, results proved that both equilibrium and non-equilibrium models have the same accuracy into predicting the variation of pressure and temperature in vertical and horizontal LNG tanks. Furthermore, as previously mentioned in section 2.4, the study developed by Felipe Huerta and Velisa Vesovic [37] shows that  $Q_{vl}$  only contributed to 0.01% of the heat ingress which can be considered negligible for an almost full tank, in our case 80% liquid filling level.

For this reason, our study will treat the stored LNG as a fuel being under a thermal equilibrium state where vapor and liquid temperatures are equal for the 80% filling level whereas a non-equilibrium approach for the other 2 filling levels will be used.

### 3.2 Mass Balance Analogy

The change in the masses of liquid and vapor natural gas can be attributed to the evaporation and condensation phenomena happening at the vapor liquid interface and can be calculated using

$$\dot{m}_{lv} = (\dot{m}'_{evap} - \dot{m}'_{cond})V \text{ [kg/s]}$$

(14)

where  $V$  represents the liquid and vapor volumes involved in the evaporation and condensation processes and is found by this equation

$$V = S_{interface} \cdot \delta$$

(15)

where,  $S_{interface}$  is the area ( $m^2$ ) of the liquid and  $\delta$  ( $m$ ) the vapor thickness that are both affected during the evaporation and condensation. For our work, the thickness of the vapor is considered to be 0.005 m according to experiments conducted by Beduz and Scurlock [47].

In order to evaluate the evaporation and condensation rates at the liquid vapor interface with respect to  $T_{sat}$  the saturation temperature, the Lee model [48] is applied. The saturation temperature being the temperature at which the liquid evaporates for a corresponding saturation pressure, the two of them being related using Antoine equation:

$$\log\left(\frac{P}{10^5}\right) = A_1 - \frac{B_1}{C_1 + T_{sat}}$$

(16)

$A_1, B_1$  and  $C_1$  are methane specific coefficients equal to 3.9895, 443.028 and -0.49 respectively [46].

$$\text{If } T_l > T_{sat} \text{ then } \quad \dot{m}_{evap} = fe \cdot \rho_l \cdot \frac{T_l - T_{sat}}{T_{sat}} \quad [kg/(m^3 s)]$$

(17)

$$\text{If } T_v < T_{sat} \text{ then } \quad \dot{m}_{cond} = fc \cdot \rho_v \cdot \frac{T_{sat} - T_l}{T_{sat}} \quad [kg/(m^3 s)]$$

(18)

$f_e$  and  $f_c$  are the evaporation and condensation coefficients respectively, set to 0.1 in this study to maintain the saturation temperature difference of both phases below 3°C [49].

### 3.3 Energy Balance Analogy

Heat balance in the liquid and vapor phases are expressed as the following:

$$\frac{dH_l}{dt} = \dot{Q}_{l,wall} + \dot{Q}_{vl} - h_v \cdot \max(\dot{m}_{lv}) + h_l \cdot \min(\dot{m}_{lv}) + V_l \frac{dP}{dt} \quad (19)$$

$$\frac{dH_v}{dt} = \dot{Q}_{v,wall} - \dot{Q}_{vl} + h_v \cdot \max(\dot{m}_{lv}) - h_l \cdot \min(\dot{m}_{lv}) + V_v \frac{dP}{dt} \quad (20)$$

Where  $H_l$  and  $H_v$  represent the total enthalpy of the liquid and vapor phases, respectively.  $\dot{Q}_{l,wall}$  and  $\dot{Q}_{v,wall}$  represent the heat transfer rate from the tank walls to the liquid and vapor phases, respectively.  $\dot{Q}_{vl}$  is the heat transfer rate between both phases at the interface and  $h_l$  and  $h_v$  represent the specific mass enthalpy of liquid and vapor phases at a specific T and P, respectively. Applying the finite difference discretization method the previous equations can be expressed as:

$$\frac{H_l^{t+\Delta t} - H_l^t}{\Delta t} = \dot{Q}_{l,wall} + \dot{Q}_{vl} - h_v \cdot \max(\dot{m}_{lv}) + h_l \cdot \min(\dot{m}_{lv}) + V_l^t \frac{P^t - P^{t-\Delta t}}{\Delta t} \quad (21)$$

$$\frac{H_v^{t+\Delta t} - H_v^t}{\Delta t} = \dot{Q}_{v,wall} - \dot{Q}_{vl} + h_v \cdot \max(\dot{m}_{lv}) - h_l \cdot \min(\dot{m}_{lv}) + V_v^t \frac{P^t - P^{t-\Delta t}}{\Delta t} \quad (22)$$

This way  $H_l^{t+\Delta t}$  and  $H_v^{t+\Delta t}$  can be calculated at time step  $t + \Delta t$ . Also, the specific mass enthalpies of both phases can be calculated from equations ( 23) and ( 24),

$$h_l^{t+\Delta t} = \frac{H_l^{t+\Delta t}}{m_l^{t+\Delta t}} \quad (23)$$

$$h_v^{t+\Delta t} = \frac{H_v^{t+\Delta t}}{m_v^{t+\Delta t}} \quad (24)$$

The following equations provide the temperatures of liquid and vapor phases at  $t + \Delta t$ :

$$\int_{T_l^t}^{T_l^{t+\Delta t}} C_{p,l} dT = h_l^{t+\Delta t} - h_l^t \quad (25)$$

$$\int_{T_v^t}^{T_v^{t+\Delta t}} C_{p,v} dT = h_v^{t+\Delta t} - h_v^t \quad (26)$$

To solve equations ( 25) and ( 26),  $T_l^{t+\Delta t}$  and  $T_v^{t+\Delta t}$  are found using the Newton-Raphson method at the  $i$ th iteration:

$$T_{l,i+1}^{t+\Delta t} = T_{l,i}^{t+\Delta t} - \frac{h_l(T_{l,i}^{t+\Delta t}) - h_l^{t+\Delta t}}{c_{p,l}(T_{l,i}^{t+\Delta t})} \quad (27)$$

$$T_{v,i+1}^{t+\Delta t} = T_{v,i}^{t+\Delta t} - \frac{h_v(T_{v,i}^{t+\Delta t}) - h_v^{t+\Delta t}}{c_{p,v}(T_{v,i}^{t+\Delta t})} \quad (28)$$

Initially, the values of  $T_l^{t+\Delta t}$  and  $T_v^{t+\Delta t}$  are  $T_{l,0}^{t+\Delta t} = T_l^t$  and  $T_{v,0}^{t+\Delta t} = T_v^t$ . In order to compute  $h_l(T_{l,i}^{t+\Delta t})$  the enthalpy of the liquid phase, one must integrate the specific heat capacity given by equation (4) with respect to the reference temperature. For the vapor phase enthalpy  $h_v(T_{v,i}^{t+\Delta t})$ , one must use equation (13) that derives from the Peng-Robinson equation of state. When the absolute values of  $T_{l,i+1}^{t+\Delta t} - T_{l,i}^{t+\Delta t}$  and  $T_{v,i+1}^{t+\Delta t} - T_{v,i}^{t+\Delta t}$  reach  $10^{-3}K$  equations ( 27) and ( 28) are converged.

### 3.4 Heat Transfer through Tank Shell

Logically speaking, the surrounding heat can enter the LNG tank through the roof, the bottom slab and the lateral walls.

#### 3.4.1 Bottom

In industrial applications, the bottom slab of storage tanks is either maintained at a constant temperature or being heated regularly using an electrical heater in order to regulate the temperature

and prevent ground freezing. Thus, in this study, the heat transfer through the bottom is taking place with a constant feeding temperature equal to the surrounding one  $T_{bottom} = T_{o,bottom\ wall,l} = 298.15K$ . Also, insulating materials of the tank bottom must have a load bearing capacity as well as suitable thermal properties. To enhance the thermal resistance, a thin layer of plywood and sand is installed between the main insulation and the nickel steel tank. Details concerning the thickness and thermal conductivity of the insulation materials covering the bottom of tank are explained in chapter 4 Table 3. The inner bottom wall temperature is assumed to be  $T_{i,bottom\ wall,l} = 123.2K$ , which is convenient for a tank with insulations having low thermal conductivities as in the case of the non-equilibrium thermodynamic model studied by Wang et al.[44].

### 3.4.2 Roof

As for the roof, the inner face of the concrete part is not in direct contact with the cryogenic atmosphere. This is due to the presence of the suspended deck along with its insulation. Therefore, predicting the inner face temperature of the roof requires one of 2 alternatives either considering a conduction-radiation-conduction approach (radiation taking place between the roof hangers) or a pure conduction approach neglecting the radiation effect. In both cases, the inner roof section is separated from the rest of the tank by a suspended deck followed by several insulating materials (see Table 3), and  $T_{o,roof\ wall} = 298.15K$  while the inner roof temperature is assumed to be  $T_{i,roof\ wall,v} = 123.2K$  equal to the inner wall temperature [44].

### 3.4.3 Walls

The heat ingress through the tank shell is also assigned to the one entering through the tank walls to the liquid and vapor phases from the environment. Assuming no heat is accumulated in

the tank wall, conjugate heat transfer can be neglected. Usual industrial performance requires to precondition the inner wall before filling the LNG until the wall temperature reaches a constant value [50]. In the preconditioning process the tank's outer wall is on direct contact with air, thus steady state heat transfer in the tank wall occurs and neglecting conjugate heat transfer will lead to a slight overestimation of the heat entrance to the vapor phase. For this reason, it is better to consider that heat enters the outer wall by natural convection from air at first, then goes through the insulation materials in the radial direction by conduction until reaching the inner wall. In the end, natural convection takes place and heat is transferred to the two phases. As convection and conduction mechanisms are both present, the heat transfer mechanism can be seen in Figure 13, the heat transfer rate through the walls can be expressed by using an equivalent resistance-capacitance network.

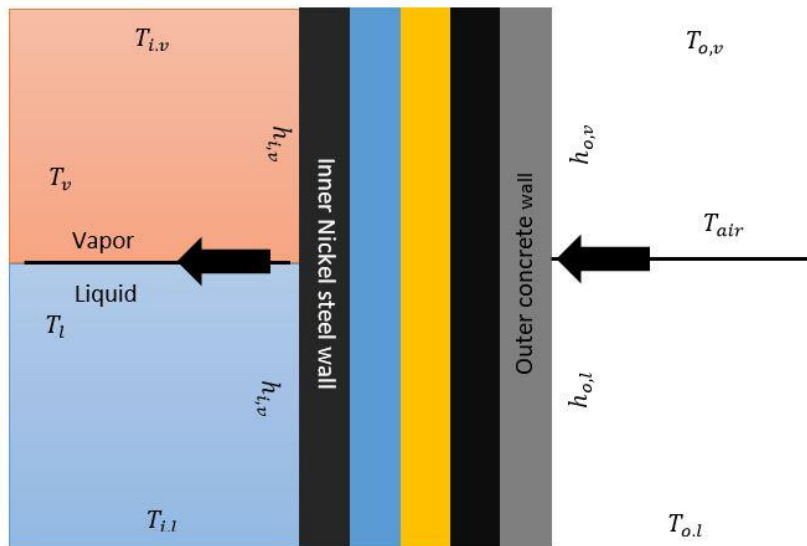


Figure 12 Heat Transfer from the Environment to Liquid and Vapor Phases through Tank Wall

The resistance-capacitance network can be solved using Kirchhoff's circuit law approach [52]. Thus the outer wall temperature of the tank in contact with the liquid and vapor phases at time  $t + \Delta t$  can be expressed as,

$$T_{o,v}^{t+\Delta t} = \frac{\left(\frac{T_{0,v}^t}{\Delta t}\right) C_1 + \frac{T_{air}}{R_1} + \frac{T_{i,v}^{t+\Delta t}}{R_2} + \frac{T_{o,roof,v}^t}{R_3} + \frac{T_{o,l}^t}{R_4}}{\frac{C_1}{\Delta t} + \frac{1}{R_1} + \frac{1}{R_2} + \frac{1}{R_3} + \frac{1}{R_4}} \quad (29)$$

$$T_{o,l}^{t+\Delta t} = \frac{\left(\frac{T_{0,l}^t}{\Delta t}\right) C_2 + \frac{T_{air}}{R_5} + \frac{T_{i,l}^{t+\Delta t}}{R_6} + \frac{T_{o,bottom,l}^t}{R_7} + \frac{T_{o,l}^t}{R_4}}{\frac{C_2}{\Delta t} + \frac{1}{R_5} + \frac{1}{R_6} + \frac{1}{R_7} + \frac{1}{R_4}} \quad (30)$$

Then, the inner wall temperatures in contact with the two phases can be explicitly calculated as,

$$T_{i,v}^{t+\Delta t} = \frac{\left(\frac{T_{i,v}^t}{\Delta t}\right) C_3 + \frac{T_{o,v}^{t+\Delta t}}{R_2} + \frac{T_v^t}{R_8} + \frac{T_{i,roof,v}^t}{R_9} + \frac{T_{i,l}^t}{R_{10}}}{\frac{C_3}{\Delta t} + \frac{1}{R_2} + \frac{1}{R_8} + \frac{1}{R_9} + \frac{1}{R_{10}}} \quad (31)$$

$$T_{i,l}^{t+\Delta t} = \frac{\left(\frac{T_{i,l}^t}{\Delta t}\right) C_4 + \frac{T_{o,l}^{t+\Delta t}}{R_6} + \frac{T_l^t}{R_{11}} + \frac{T_{i,bottom,l}^t}{R_{12}} + \frac{T_{i,v}^t}{R_{10}}}{\frac{C_4}{\Delta t} + \frac{1}{R_6} + \frac{1}{R_{11}} + \frac{1}{R_{12}} + \frac{1}{R_{10}}} \quad (32)$$

Heat transfer rates from the surroundings to the vapor and liquid phases of the tank walls are computed following equations ( 33) and ( 34). The summation of these two provides the total heat transfer rate to the tank

$$\dot{Q}_{v,wall} = \frac{T_{i,roof,v} - T_v}{R_{13}} + \frac{T_{i,v} - T_v}{R_8} \quad (33)$$

$$\dot{Q}_{l,wall} = \frac{T_{i,bottom,l} - T_l}{R_{14}} + \frac{T_{i,l} - T_l}{R_{11}} \quad (34)$$

The details of the thermal resistance-capacitance scheme shown in are present in appendices

### 3.5 Heat transfer rate at the liquid vapor interface

For calculation purposes, a natural convection heat transfer across the interphase has been assumed and is found by

$$\dot{Q}_{vl} = h_{vl,interface} (T_v - T_l) A_{interface} \quad (35)$$

A rigorous CFD simulation of an LNG storage tank presented by Saleem et al. [28] in 2018 where an extensive investigation has been made that takes into account internal flow dynamics and complex boiling phenomena that occur in an LNG tank, a steady state interfacial heat transfer coefficient was estimated to be  $4 \text{ W/m}^2\text{K}$  which will be used in our study.

To better understand the algorithm of solving the previously mentioned equations for the assumed thermal equilibrium state, Figure 14 presents a chart describing the flow of equations that are solved using Excel and Matlab. This flow chart has been taken from a non-equilibrium thermodynamic study on an LNG tank [44] and adapted to our study. The input parameters to this model involve the tank geometry and parameters that will be furtherly cited in Chapter 4, along

with the initial temperature and pressure of LNG tank. Also the LNG level in the tank will be set as an input parameter and will be altered between 80%, 50% and 10% liquid filling level.

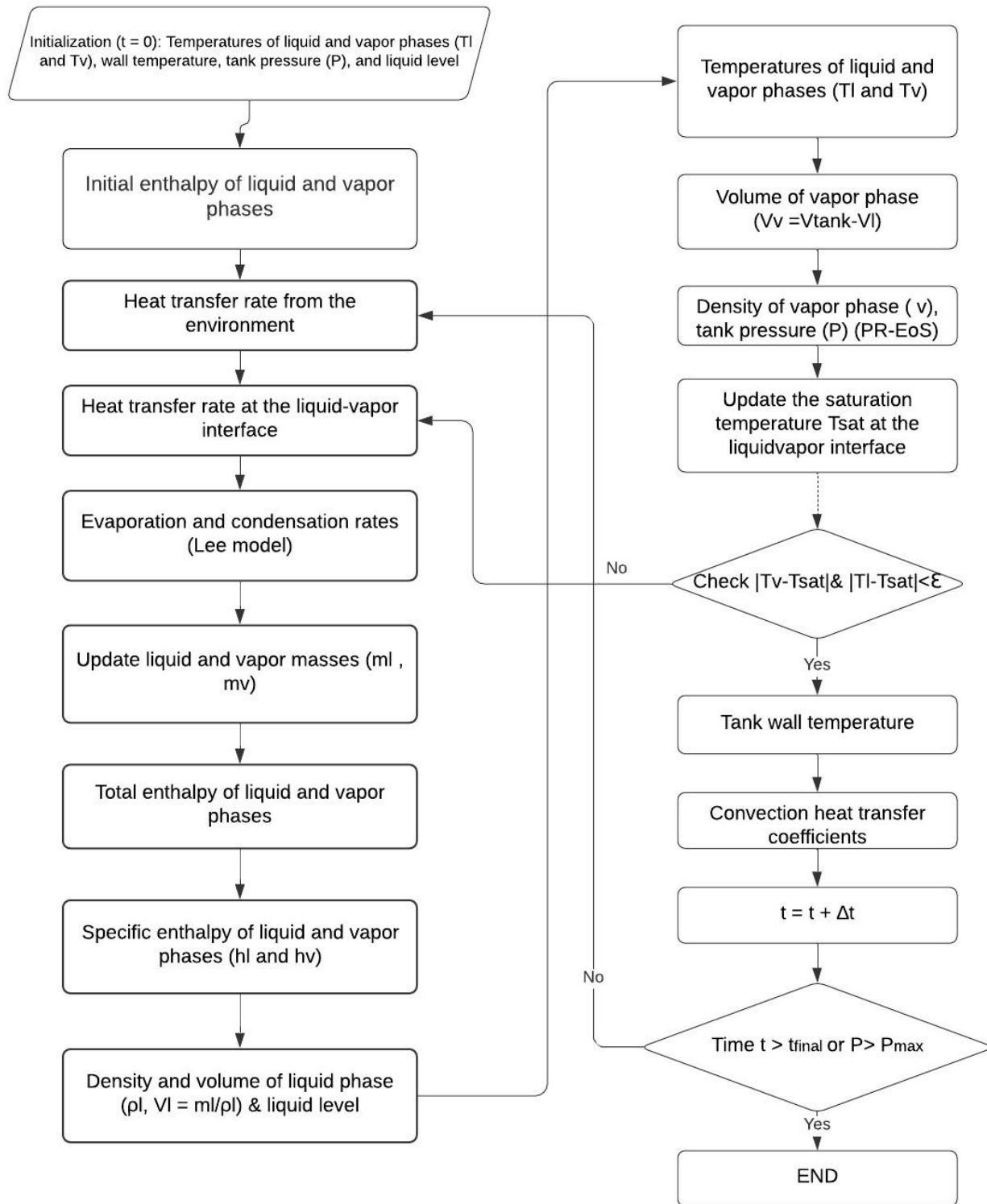


Figure 14: Flow chart for solving equations for the thermodynamic equilibrium modeling

## Chapter 4: Case Study

### 4.1 Tank Parameters and Materials

In our study, the LNG storage tank in question is a vertical above-ground double walled storage tank with a height and diameter equal to 41m and 90m, respectively. This  $2.6 \times 10^5 m^3$  is considered a huge storage tank compared to the ones currently present in the industry. As it clear in Figure 14, the inner face of the concrete roof is not in direct contact with the vapor phase above the LNG, as a suspended deck is present along with a layer of insulations that act as a thermal barrier. Concrete covers the outer side of the tank completely from the top to the bottom where an electric heater is added to prevent ground freezing. Before reaching the nickel steel inner tank a carbon steel liner covers the bottom and wall sections from the inside followed by 2 layers of load bearing glass wool, a sand layer and plywood for the bottom while on the sides an expander perlite filling and a glass wool layer are stacked. As for the top part, following the roof hangers comes the layer of expander perlite with another one made of glass wool for thermal insulation purposes. The LNG properties and tank modeling parameters are mentioned in Table 2

*Table 2: LNG storage tank modeling parameters*

Parameter	Value
Tank height ( $H$ ), (m)	41
Tank diameter ( $D$ ), (m)	90
Ambient temperature $T_{amb}$	25
Bottom temperature, ( $^{\circ}C$ )	25
Tank pressure, (bar)	1.17
Latent heat of vaporization of LNG ( $\lambda$ ), kJ/kg	510

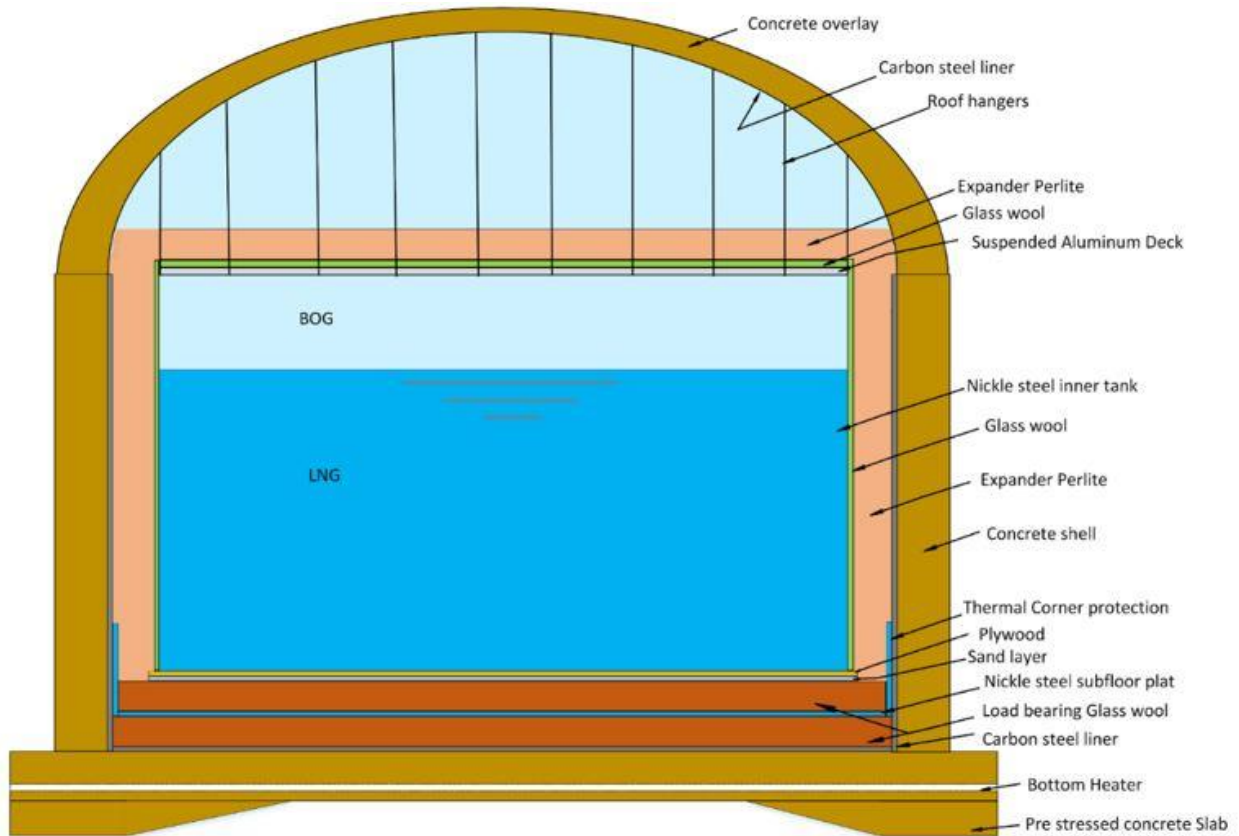


Figure 15: LNG vertical storage tank [51]

The density and specific heat values supplied by the insulation materials utilized in this LNG storage tank are listed in Table 3, while the geometrical details of the insulation layers are reported in Table 4.

Table 3: Density and Specific heat values for the insulating materials[51]

Insulating Material	Density (kg/m <sup>3</sup> )	Specific heat (kJ/kgK)
Perlite (loose)	1100	--
Perlite (expanded)	40-140	0.387
Concrete	2400	0.960
Glass wool	24	0.670
Total Insulation	1331.7	0.783
Ni-Steel	7801	0.456

*Table 4. 1 Thickness of tank wall materials[51]*

<b>Elements of shell</b>	<b>Thickness (m)</b>	<b>Thermal conductivity (W/m.K)</b>
Nickel steel tank	0.02	90.2
Glass fiber	0.15	0.03
Perlite	0.9	0.038
Concrete overlay	1	1.8

*Table 4. 2 Thickness of tank roof materials [51]*

<b>Elements of Roof</b>	<b>Thickness (m)</b>	<b>Thermal conductivity (W/m.K)</b>
Nickel steel tank	0.02	90.2
Suspended aluminum	0.003	-
Glass fiber	0.15	0.03
Perlite	0.9	0.038
Steel liner	0.005	90.2
Concrete overlay (8 inches)	0.203	1.8

*Table 4. 3 Thickness of tank bottom materials [51]*

<b>Elements of Bottom</b>	<b>Thickness (m)</b>	<b>Thermal conductivity (W/m.K)</b>
Nickel Steel	0.02	90.2
plywood	0.012	-
Sand layer	0.005	-
Load bearing rigid cellular glass fiber	0.5	0.03
Nickel Steel subfloor plate	0.02	90.2
Load bearing rigid cellular glass fiber	0.5	0.03
Carbon steel liner	0.001	42.6
Concrete slab heater	2	1.8

## 4.2 Numerical Development

Having mentioned the tank materials and parameters, we start by setting on Matlab the initial pressure of the tank  $P_{tank} = 1.17bar = 117000Pa$ . Then using Antoine's equation we can compute  $T_{sat}$  that is equivalent to the initial liquid and vapor temperatures for the 80% liquid filling level case (Thermodynamic equilibrium). For such pressure, liquid and vapor temperatures were found to be  $T_v = T_l = 116.087K$ . As for the other two filling levels, the increase in the vapor area increases its temperature to 118.15K for the 50% filling level and to 120.15K for the 10% filling level [53].

The inner wall temperature was assumed to be  $T_{i,wall} = 123.2 K$  while the outer one is equivalent to the ambient temperature  $T_{o,wall} = 298.15 K$ . Moving forward, the liquid thermophysical properties were calculated on Matlab using the function  $f(T)$  (4) and the coefficients in Table 1, hence getting the liquid density  $\rho_l = 419.4881 kg/m^3$ , the specific heat capacity  $C_{p,l} = 3533 J/kg.K$ , the viscosity  $\mu_l = 1.07 * 10^{-4} kg/m.s$ , conductivity  $k_l = 0.1782 W/m.K$ , and thermal expansion coefficient  $\beta_l = 0.0015$ . In order to find the convection heat transfer coefficient on the side of the walls, Churchill-Chu correlation [55] for the natural convection heat transfer had to be used:

$$Nu_{av} = \frac{h_{x,wall}L_x}{k_{fluid}} = \left[ 0.825 + \frac{0.387Ra_x^{\frac{1}{6}}}{\left[1 + \left(\frac{0.492}{Pr_x}\right)^{\frac{8}{27}}\right]^{\frac{1}{4}}}\right]^2$$

(36)

Where,

$$Ra_x = \frac{g\beta_f\Delta T_x L_x}{\alpha_f \nu_f} \quad (37)$$

$$Pr_x = \frac{\nu_f}{\alpha_f} \quad (38)$$

In equations ( 36) and ( 37),  $x$  is the increment that represents the different parts of the wall. This is more explained in the Table 4

*Table 4: Variables in the calculation of the convection transfer coefficients on the wall.*

<b>x</b>	<b>Fluid</b>	<b><math>L_x</math>(m)</b>	<b><math>\Delta T_x</math>(K)</b>	<b><math>T_{ref}</math>(K)</b>
<b>Outer wall,v</b>	Air	Length of outer wall (vapor part)	$T_{air} - T_{o,wall,v}$	$0.5(T_{air} + T_{o,wall,v})$
<b>Outer wall,l</b>	Air	Length of outer wall (liquid part)	$T_{air} - T_{o,wall,l}$	$0.5(T_{air} + T_{o,wall,l})$
<b>Inner wall,v</b>	Vapor phase	Length of inner wall (vapor part)	$T_{i,wall,v} - T_v$	$0.5(T_{i,wall,v} + T_v)$
<b>Inner wall,l</b>	Liquid phase	Length of inner wall (liquid part)	$T_{i,wall,l} - T_l$	$0.5(T_{i,wall,l} + T_l)$

*Table 5: Summary of the different initial temperatures*

<b>Temperatures (K)</b>	
$T_{air}$	298.15 (given)
$T_{o,wall,v}$	298.15 (set at the ambient temperature)

$T_{o,wall,l}$	298.15 (set at the ambient temperature)
$T_v$ [53]	116.087 (80%), 118.15(50%), 120.15(10%)
$T_l$	116.087
$T_{i,wall,v}$	123.2 (assumed)
$T_{i,wall,l}$	123.2 (assumed)

Also,  $\beta_f$ ,  $\alpha_f$  and  $\nu_f$  are the thermal expansion coefficient, thermal diffusivity ( $m^2/s$ ) and kinematic viscosity ( $m^2/s$ ) of the LNG at  $T_l$ , respectively.  $g$  is the gravity acceleration  $9.81(m^2/s)$ .

$$\alpha_f = \frac{k}{\rho C_p} \quad (39)$$

$$\nu_f = \frac{\mu}{\rho} \quad (40)$$

In fact,  $L_x$  is calculated following this formula:

$$L_x = \frac{V_{tank} * Filling\ level\ \%}{\pi * r^2} \quad (41)$$

Table 6: Height of liquid and vapor phases for the three different liquid filling levels

Filling level	$L_{liq}(m)$	$L_{vap}(m)$
80%	32.69	8.304
50%	20.43	20.565
10%	4.08	36.913

The heat transfer coefficients at the wall for the 80%, 50% and 10% liquid filling levels (LFL) for the two phases were calculated on Matlab and are presented in Table 7

Table 7: Rayleigh number and heat transfer coefficients ( $W/m^2.K$ ) for the different parts of the wall

	80% filling level	50% filling level	10% filling level
$Ra_{outer\ wall,v}$	0	0	0
$Ra_{outer\ wall,l}$	0	0	0
$Ra_{inner\ wall,v}$	117.324	206.276	223.615
$Ra_{inner\ wall,l}$	461.917	288.698	57.739
$h_{outer\ wall,v}$	0.015	0.006	0.003
$h_{outer\ wall,l}$	0.004	0.006	0.029
$h_{inner\ wall,v}$	93.506	45.470	26.016
$h_{inner\ wall,l}$	37.311	51.124	150.479

Concerning the gas phase, using the PR-EoS on Matlab,  $P_{gas}$  was found to be equal to 0.397, 0.439 and 0.457 bar for the 80%, 50% and 10% liquid filling levels, respectively. In order to find  $h_{ideal}$ ,

$C_{p,vap}$  ( $\frac{kJ}{kg.K}$ ) had to be calculated using equation ( 42)

$$C_{p,vap} = 0.628326 \frac{T_c}{T_{vap}} + 0.752532 + 0.582779 \frac{T_{vap}}{T_c} + 0.082044 \left( \frac{T_{vap}}{T_c} \right)^2 - 0.010773 \left( \frac{T_{vap}}{T_c} \right)^3$$

(42)

Multiplying this value by the molecular weight of CH<sub>4</sub> will give  $C_{p,vap} \left( \frac{kJ}{mol.K} \right) = 0.035$  for the 80% LFL, 0.034 and  $0.033 \frac{kJ}{mol.K}$  for the 50%LFL and 10%LFL, respectively. Then  $h_{ideal}$  was calculated for the three LFL hence the molar vapor enthalpies for the 80%, 50% and 10% liquid filling levels were found to be  $9.34 \times 10^6$ ,  $10.32 \times 10^6$  and  $10.73 \times 10^6$  kJ/mol, respectively.

As for the heat transferred from the environment to the tank, as previously mentioned following a resistance capacitance network, the thermal resistances were calculated for the outer and inner parts of the tank through the top, bottom and walls in contact with the two phases and are presented in and Appendix A.2. These values were calculated on excel for the three different liquid filling levels and taking into consideration the insulation thicknesses and thermal conductivities of the different materials, as well as the multiple heat transfer coefficients that were calculated Table 7 for the inner and outer parts of the tank. Moreover, the thermal capacitances were calculated using the information provided in Appendix A.3 and are presented in **Appendix A.2**. Thus using the thermal-capacitance network, the outer and inner wall temperatures in contact with the two phases for the three liquid filling levels were calculated using equations ( 29), ( 30), ( 31) and ( 32) with a time step of  $\Delta t = 60s$ . These values are presented in Table 8

*Table 8: Inner and outer wall temperatures in contact with the liquid and vapor phases for the three different liquid filling levels*

	$T_{o,v}^{t+\Delta t}$	$T_{i,v}^{t+\Delta t}$	$T_{o,l}^{t+\Delta t}$	$T_{i,l}^{t+\Delta t}$
<b>80% liquid filling level</b>	297.86	<b>123.38</b>	297.86	<b>123.97</b>

<b>50% liquid filling level</b>	297.86	<b>123.82</b>	297.86	<b>123.43</b>
<b>10% liquid filling level</b>	297.86	<b>124.36</b>	297.86	<b>122.05</b>

It is possible then to calculate the heat transfer rates from the surroundings to the vapor and liquid phases of the tank walls using equations ( 33) and ( 34). These results are presented in Table 9 below along with the heat transfer rate ( 35) at the interphase for the three LFL.

*Table 9: Heat Leakage, BOG and BOR for the three LFL*

<b>Data Calculated</b>	<b>80% LFL</b>	<b>50% LFL</b>	<b>10%LFL</b>
Heat leak from tank roof (kW)	22.9	22.3	16.8
Heat leak from tank bottom (kW)	33.8	33.6	33.3
Heat leak from tank vapor area (kW)	8.31	26.9	42.23
Heat leak from tank liquid area (kW)	25.94	20.69	9.9
Heat leak from vapor to liquid (kW)	0	43.58	55.07
Liquid level in the tank h (m)	32.7	20.43	4.09
Wall side liquid contact area (m <sup>2</sup> )	9244.44	5777.77	1155.55
Wall side vapor contact area (m <sup>2</sup> )	2348.032	5814.699	10436.921
Liquid temperature (K)	116.087	116.087	117.543

Vapor temperature (K)	116.087	118.15	120.15
Total ambient heat leak to the tank (kW)	90.95	103.49	102.23
Total heat leak to liquid (kW)	59.74	97.87	98.27
BOG rate (kg/h)	421.69	690.84	693.67
Mass total LNG	87152000	54470000	10894000
BOR (wt%)	0.012	0.03	0.152

---

### 4.3 Model Results

The scenarios of 80%, 50% and 10% were considered as references for a full containment tank, half-filled tank and quasi-filled tank. Estimating BOG for other levels requires some variations in the thermal-resistance capacitance model

#### 4.3.1 Tank filled with 80% LNG

As previously mentioned, the 80% LFL case assumes a thermodynamic equilibrium between the liquid and vapor phases. This assumption is reasonable because the small vapor space created from the displacement of the hot vapor by the cold LNG is filled by the BOG produced. The total heat leak from the environment to this tank is 85.35 kW, this heat being transferred from the tank roof, bottom and walls. As for the heat leak to the liquid part of the tank which comes from the vertical wall and bottom part in contact with the liquid phase in addition to the vapor to liquid heat transfer was found to be 59.74kW. Since the BOG generated refers to the liquid vaporization rate, it is wrong to attribute the total heat leak to the tank as the ultimate contributor to BOG generation. In fact this value will be over-predicted by 52% which is huge and also a common mistake in a lot of studies. For this reason, taking into consideration the heat leak to the liquid is the right way to

find the BOG which is 429.61 kg/h leading to a BOR (% of liquid vaporization of the total liquid volume per day) of 0.012%/day which is way less than normal conditions 0.15%/day as stated in section 2.3

#### **4.3.2 Tank filled with 50% LNG**

For a 50% LFL tank, heat leak from the vapor part is bigger since for such level, more vapor area is provided for heat to be transferred compared to the 80% LFL. The vapor temperature is then increased to 118.15K which can be attributed to the higher heat capacity of LNG. Thus the temperature difference between the liquid and vapor phases is somehow considerable ( $\approx 2\text{K}$ ) and causes around 88.5% of the heat ingress to the vapor phase to be transferred to liquid phase via the vapor liquid interphase. If all heat leakage to the tank is assigned to the BOG generation, the BOG will be over-predicted by 5.7% which is way smaller than the over-prediction of the 80% LFL case, due to the vapor liquid heat transfer at the interface that contributes to the liquid heat leak and therefore the BOG. At this heat transfer rate, the tank BOR is 0.03%/day which is also within the safe margin.

### 4.3.3 Tank filled with 10% LNG

In the case of 10%LFL tank, heat leak to the vapor is even bigger compared to the other two cases, where the vapor temperature is further increased to 120.15K. With the tank almost full of vapor NG, almost all of the heat entering the tank is transferred to the liquid phase resulting in a high BOG rate equal to 693.67 kg/h and therefore a BOR of 0.152%/day which exceeds the stated normal threshold by a very small percentage, thus is not considered very risky. However, a long storage period at this liquid filling level needs to be treated by refilling the tank since at some point the BOG collector will not be able to withstand large quantities before sending them to the recondenser which may cause pressure build-up.

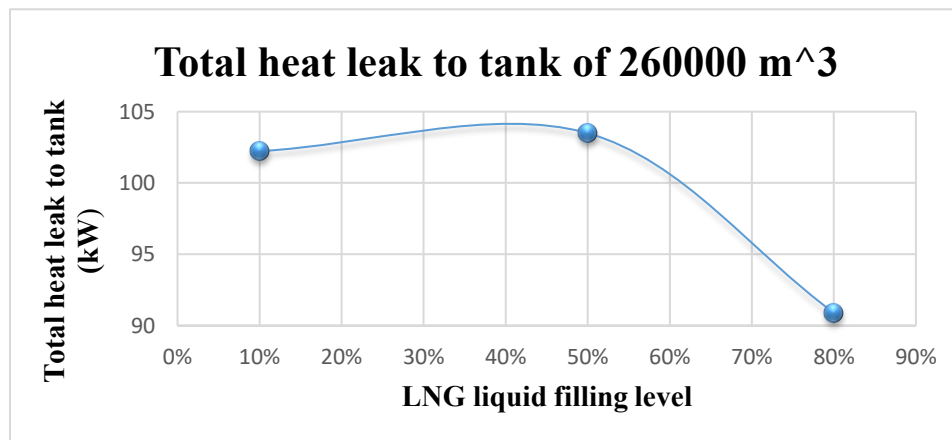


Figure 16: Total heat leak to the tank

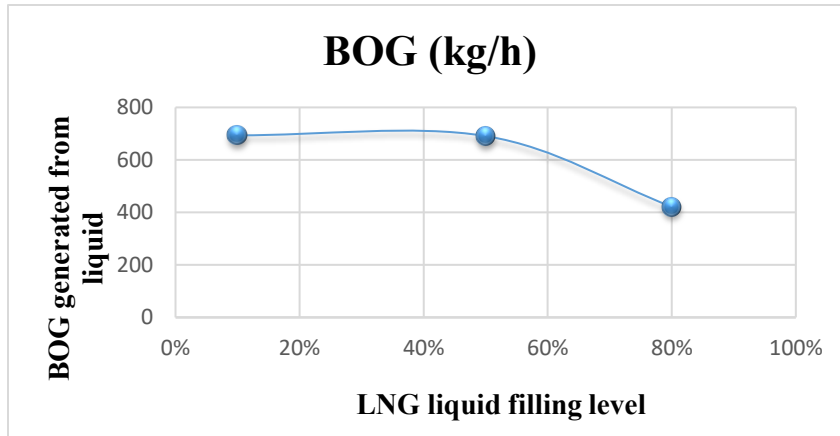


Figure 17: BOG from liquid heat leak

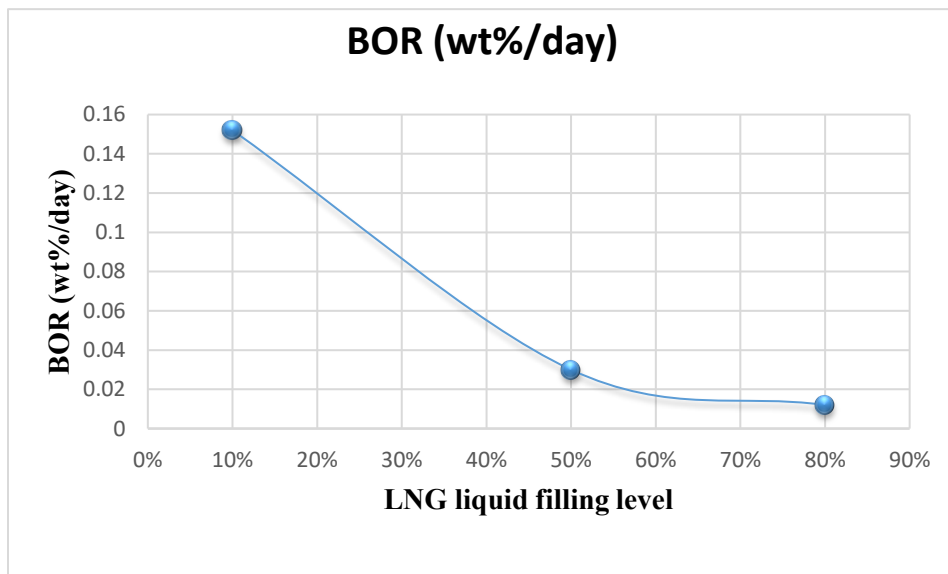


Figure 18: BOR from heat leakage to tank

#### 4.4 Discussion

As previously mentioned, BOR is defined as the LNG vaporized per day of the total liquid mass present in the tank. Frequently, the operator or vendor assigns a gross value of 0.05wt% for the maximum tank filling level as the BOR. This assumption is reliable in the case where the total heat leakage into the tank is constant (static BOR), and unrelated to the liquid filling level inside. This

can be seen in Figure 16 where for each LNG volume inside the tank a specific heat transfer rate can be attributed, and only a 12% increase in the total heat ingress is present between the 80% and 10% LFL. However, this assumption does not highlight the fact that heat is distributed between the liquid and vapor phases, and the effect of the liquid level variation on the BOG and BOR which needs to be addressed.

It is evident now that the BOR is not static even though the total heat ingress to the tank is nearly constant, instead it is strongly dependent on the liquid filling level inside the tank.

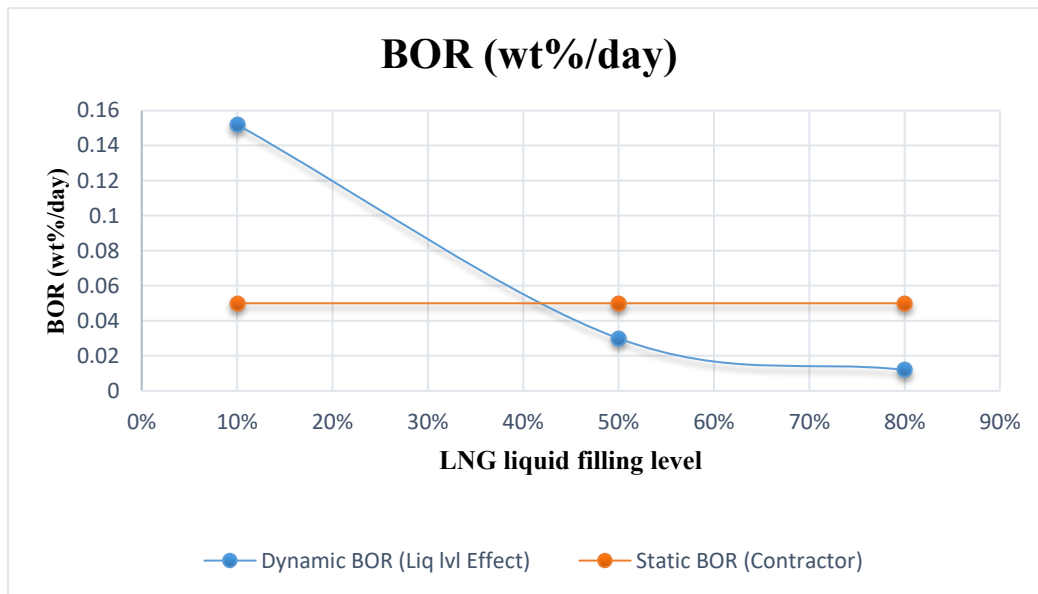


Figure 19: Static vs Dynamic BOR in LNG tank

Upstream units such as recondensers and compressors should be designed taking into consideration the dynamic BOR instead of the static one for accurate BOG handling. In other words, adequate preparation is required to address BOG based on the worst case scenario (high BOR), such does this work by studying the 10% LFL.

#### 4.5 Comparison with previous results

In numerous studies, conduction and convection heating models were run to estimate heat ingress to LNG storage tanks in order to assess the BOG generation inside, the holding time and the decrease of liquid levels on the long term. However, structural designs of LNG tanks were complicated in order to perform an accurate thermal analysis. With the use of a thermal resistance capacitance network, thermodynamic equilibrium and non-equilibrium model were implemented in a recent study by Wang et al. [44] and the results were compared with two sets of experimental data which validated the fact that non equilibrium model accurately predict the thermophysical properties of the tank under dynamic operating conditions. Similarly in our study, this non-equilibrium model was used for two LFL (50% and 10%) while for the 80% case, the thermodynamic equilibrium model was the proper choice for an almost full tank, with vapor and liquid having the same temperature (initial conditions). In another study that tackles the BOG prediction and the BOR in an LNG storage tank [51] having the same parameters and geometry as our study, it was proven that the total heat transfer to the tank practically remains constant which also validates our results. Moreover, over-prediction cases of BOG were analyzed whenever the heat leak is completely assigned to the liquid phase, which aligns with what resulted from our study, that vapor temperature increases and this unequal distribution of heat in both phases will alter the BOG. The following graph visualizes a comparison between the BOR in the Khan et al.[51] study and this present one:

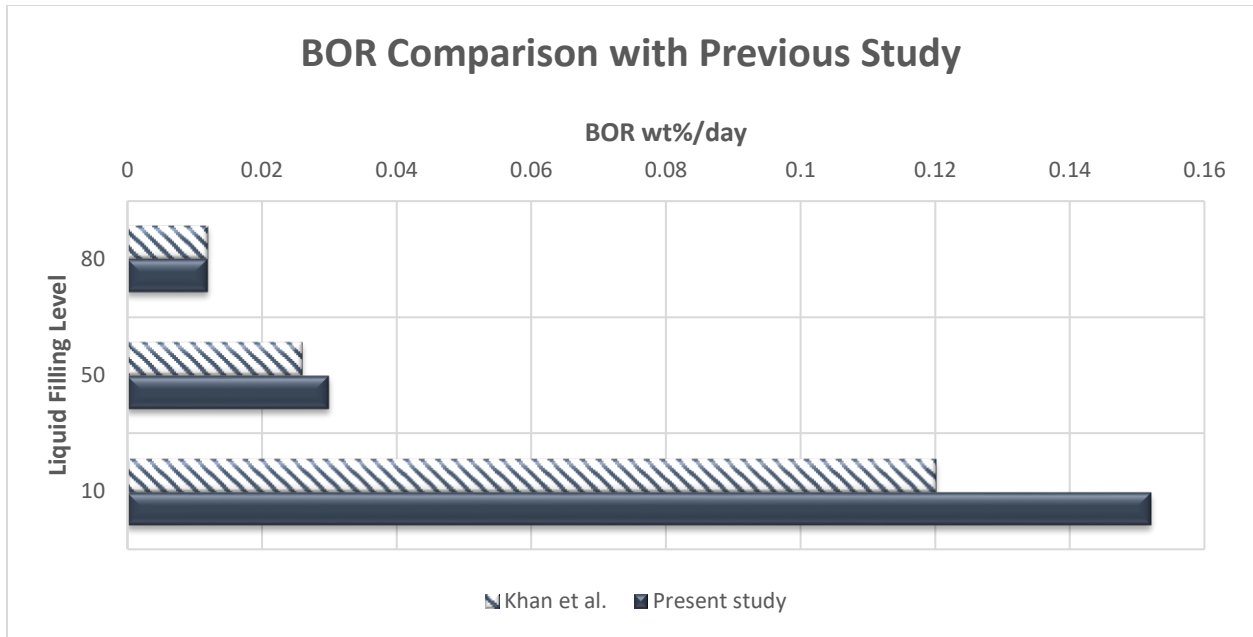


Figure 20: BOR comparison chart between previous and current study

This graph clearly shows that both studies predicted almost the same BOR for the two initial liquid filling levels. However, for the 10% LFL a slight variation in the BOR is observed. This is due to the fact that the thermal resistance capacitance network used in our study gave a more accurate prediction of the heat transferred to the tank especially from the bottom slab where in our case from this part of the tank the heat ingress to the liquid phase was considerably higher compared to the previous study. Nevertheless, the results in the present study are consistent with the work of previous ones. The major difference comes with the method used to assess the thermal performance of the tank.

## Chapter 5: Environmental aspect of technology presented

In the recent years, the LNG industry witnessed an incessant drift towards being more cost effective, while improving land area use by providing large tanks to host the continuous increase of the gross capacity of ocean carriers [56]. From an environmental point of view, reducing carbon footprint of storage tank from a life cycle perspective is also considered an on-going achievement. While the vertical tank is assumed to be rested on a horizontal surface, a critical carbon assessment

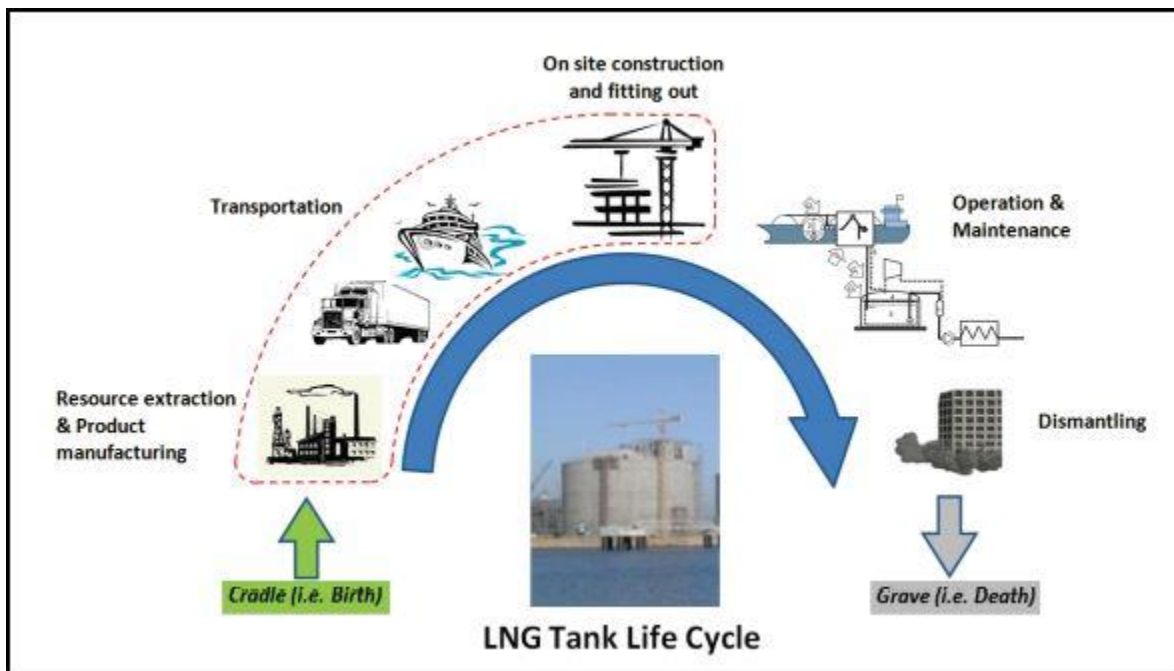


Figure 21: Tank Life Cycle [56]

takes place from the very moment raw materials of the tank are extracted until operation is reached and finally the dismantling occurs. Figure 21 gives a better understanding of the LNG tank life cycle from cradle to grave.

The carbon footprint (CF) of such technology takes into account the contribution of the different steps, their environmental impact and can be calculated as follows:

$$CF = CF_{manufacturing} + CF_{transportation} + CF_{construction} + CF_{O\&M/Dismantling} \quad (43)$$

Maintenance of a static storage tank (present study) is non-existent or negligible. Manufacturing of the materials, their transportation and the final construction of the tank contribute the most to the carbon emissions. While the carbon footprint of the manufacturing is calculated following equation (44) along with the information presented in Table 10, its calculation for the two other next steps was not done in this study for the lack of information such as the location and travelling distances of the materials as well as the workers.

$$CF_{manufacturing} = \sum iW_i * F_i \quad (44)$$

Where  $W_i$  is the material weight and  $F_i$  is the per unit global warming potential in ton CO<sub>2</sub>-eq for the production of 1 ton of the material.

The following table summarizes these two parameters

Table 10: Parameters used for the manufacturing CF calculation

Tank Section	Type of material	Material grade	Volume (m <sup>3</sup> )	Density(kg/m <sup>3</sup> )	Mass (ton)	Per unit global warning potential in tons CO <sub>2</sub> -eq
Concrete Tank	Concrete Roof	Concrete	1292.7	2400	3102	1.7
	Concrete Walls		5482.865		13158	1.7
	Prestressed Concrete Slab		12723.450		30536	1.7
In tank	Metals	Carbon Steel	38.16	7850	299	1.7
		Nickel Steel	439.42	7801	3427	2.3
		Aluminum	17.36	2710	47	8
	Insulation	Perlite	10091	90	908.19	-
		Glass Fiber	5789.71	24	138.95	1.6

Therefore the manufacturing CF for the LNG tank in this study is equivalent to 88,541 carbon in tons CO<sub>2</sub>-eq.

### **5.1 Future improvements and limitations**

A proper estimation of the tank's BOR for the three different liquid filling levels has been carried out in this study after finding the heat leakage from the tank's roof, bottom and walls and its proper distribution among the vapor and liquid phases. However, it should be noted that this study is being performed assuming an average ambient temperature of 25°C, which is not always the case. In fact, heat leaking from the outside can always be either higher or lower depending on weather conditions, where temperatures vary as well as day and night conditions. Also, the LNG composition is mainly considered as pure methane, or light LNG for calculation purposes. However, sometimes stored LNG can be containing ethane, propane and also nitrogen to further drop its boiling temperature. Moreover, normal operations are not taken into consideration such as active filling of the tank or discharge of LNG into loading trucks or carriers. The tank is considered to be closed and under static conditions for the three different filling levels, therefore heat ingress is the only contributor to the BOG generation. Therefore, the thermal design in this study can act as a starting stage for further heat leakage projects by simply changing the initial thermophysical properties depending on the LNG content and the operating conditions. On the other hand, having found that for a low liquid filling level, a higher BOG is induced. This study provides a basis for accurate BOG and BOR calculations to further address the situation and avoid hazardous problems.

## Chapter 6: Conclusion

In this study, an equilibrium and non-equilibrium thermodynamic approach were developed depending on three different liquid fillings of an LNG tank using a resistance-capacitance network. After investigating the thermal performance of the tank including the heat transferred from the environment at an average temperature of  $25^{\circ}\text{C}$  by natural convection and conduction through the insulating materials, the total heat ingress to the tank turned out to be barely changing with the different filling levels. The results showed that for an 80% liquid level, the heat leak is mostly attributed to the liquid part of the tank resulting in a BOR of  $0.012\text{wt\%/day}$ . Instead, a 50% filled tank, where heat leak is almost equivalent between the two phases, results in a BOR of  $0.03\text{wt\%/day}$  noting that a vapor liquid heat transfer happened at the interface. Similarly for a 10% filled tank, while reasonably heat leak should be attributed to the abundant vapor phase, heat transferred to liquid is nonetheless the biggest; this is due to the interface heat transfer. For this filling level a BOR of  $0.152\text{wt\%/day}$  was found which may on the long term exceed the ventilating ability of the storage tank resulting in pressure build-up and hazardous effects. Furthermore, results showed that heat ingress is not fully happening to the liquid phase and heat leakage occurs at the different parts of the tank disregarding the fluid phase. However, BOG calculation is linked properly to the liquid heat ingress instead of the total one or an over-prediction of the BOR will happen. It is therefore important to say that BOR strongly depends on the liquid level of the tank, the heat distribution between the liquid and vapor phases but also the interface heat transfer. This goes to say that for a low liquid level, BOG is under-predicted using a static BOR approach.

Environmentally speaking, with the data provided, the manufacturing carbon footprint of the  $260000\text{ m}^3$  LNG storage tank was calculated and found to be 88,541 carbon in tons  $\text{CO}_2\text{-eq}$ .

More data is required for an accurate estimation of the total carbon footprint and emissions of this technology.

## Appendices

### Appendix A.1: Details of the thermal resistance (K/W) network

Description	Definition	Eq.
Inner convection resistance on top wall	$R_{13} = \frac{1}{h_{i,inner\ top\ wall,v} * A_{inner\ top\ wall,v}}$	A.1
Outer convection resistance on the wall in contact with vapor space	$R_1 = \frac{1}{h_{i,outer\ wall,v} * A_{i,outer\ wall,v}}$	A.2
Conduction resistance on the wall in contact with the vapor space due to insulation	$R_2 = \frac{1}{A_{i,outer\ wall,v}} \sum \frac{t}{k}$	A.3
Inner convection resistance on the wall in contact with vapor phase	$R_8 = \frac{1}{h_{i,inner\ wall,v} * A_{i,inner\ wall,v}}$	A.4
Outer convection resistance on the wall in contact with liquid phase	$R_5 = \frac{1}{h_{i,outer\ wall,l} * A_{i,outer\ wall,l}}$	A.5
Conduction resistance on the wall in contact space due to insulation	$R_6 = \frac{1}{A_{i,outer\ wall,l}} \sum \frac{t}{k}$	A.6
Inner convection resistance on the wall in contact with liquid phase	$R_{11} = \frac{1}{h_{i,inner\ wall,l} * A_{i,inner\ wall,l}}$	A.7
Inner convection resistance on the bottom wall	$R_{14} = \frac{1}{h_{i,inner\ bot\ wall,l} * A_{inner\ bottom\ wall,l}}$	A.8
Conduction resistance between the outer top wall and outer vertical wall in contact with vapor phase	$R_3 = \frac{L_{i,outer,top-vertical,v}}{k_{outer\ wall} * A_{i,cross\ sect,outer,top-vertical,v}}$	A.9
Conduction resistance between inner top wall and inner vertical wall in contact with vapor space	$R_9 = \frac{L_{i,inner,top-vertical,v}}{k_{inner\ wall} * A_{i,cross\ sect,inner,top-vertical,v}}$	A.10
Conduction resistance in the outer vertical wall in contact with the liquid and vapor spaces	$R_4 = \frac{L_{vertical\ wall\ v-l}}{k_{outer\ wall} * A_{cross\ sect,outer,vertical}}$	A.11
Conduction resistance in the inner vertical wall in contact with liquid and vapor spaces	$R_{10} = \frac{L_{vertical\ wall,v-l}}{k_{inner\ wall} * A_{cross\ sect,inner,vertical}}$	A.12
Conduction resistance between outer bottom wall and outer vertical wall in contact with liquid phase	$R_7 = \frac{L_{i,outer,bottom-vertical,l}}{k_{outer\ wall} * A_{i,cross\ sect,outer,bott-vert,l}}$	A.13

Conduction resistance between inner bottom wall and inner vertical wall in contact with the liquid phase

$$R_{12} = \frac{L_{i,inner,bottom-vertical,l}}{k_{inner\ wall} * A_{i,cross\ sect,inner,bott-vert,l}}$$

A.14

*Appendix A.2: Parameters used to calculate the thermal resistances*

	80% liquid filling level	50% liquid filling level	10% liquid filling level
$h_{i,inner\ wall,v}$	93.506	45.471	26.0158
$A_{inner\ top\ wall,v}$		5788.559	
$h_{i,outer\ wall,v}$	0.0146	0.006	0.003
$A_{i,outer\ wall,v}$	2348.032	5814.699	10436.921
$A_{i,inner\ wall,v}$	2239.762	5546.577	9955.663
$h_{i,outer\ wall,l}$	0.0037	0.0059	0.029
$h_{i,inner\ wall,l}$	37.311	51.124	150.479
$A_{i,outer\ wall,l}$	9244.444	5777.778	1155.556
$A_{i,inner\ wall,l}$	8818.173	5511.358	1102.272
$A_{inner\ bottom\ wall,l}$		5788.559	
$L_{i,outer,top-vertical,v}$	106.609	131.131	163.826
$k_{outer\ wall}$		1.8	
$A_{i,cross\ sect,outer,top-vertical,v}$	8709.758	12176.424	16798.646
$L_{i,inner,top-vertical,v}$	102.459	126.981	159.676
$k_{inner\ wall}$		90.9	
$A_{i,cross\ sect,inner,top-vertical,v}$	8028.321	11335.136	15744.223
$L_{vertical\ wall\ v-l}$		38	
$A_{cross\ sect,outer,vertical}$		11592.477	
$A_{cross\ sect,inner,vertical}$		10248.81771	
$L_{i,outer,bottom-vertical,l}$	155.391	130.869	98.174
$A_{i,cross\ sect,outer,bott-vert,l}$	15606.169	12139.503	7517.281
$L_{i,inner,bottom-vertical,l}$	151.241	126.719	94.024
$h_{i,inner,top,wall}$	8.212	5.83	3.52

$h_{i,inner,bot,wall}$		8.21		
Thermal Resistance (K/W)	80% liquid filling level	50% liquid filling level	10% liquid filling level	
R13	3.104E-04	2.263E-04	1.807E-04	
R1	0.029	0.029	0.029	
R2	0.012	0.005	0.003	
R8	8.77E-04	1.97E-04	0.86E-04	
R5	0.029	0.029	0.029	
R6	0.003	0.005	0.025	
R11	3.039E-06	3.549E-06	6.029E-06	
R14	2.10E-04	2.10E-04	2.10E-04	
R3	0.006	0.006	0.005	
R9	0.0001	0.0001	0.0001	
R4	0.002	0.002	0.002	
R10	4.078E-05	4.078E-05	4.078E-05	
R7	0.005	0.006	0.007	
R12	0.0001	0.0001	0.0001	

*Appendix A.3: Masses of the inner and outer insulation layers in contact with the liquid and vapor phases*

	80% filling level	50% filling level	10% filling level
m_outer_v (kg)	2868428.835	7103415.724	12750064.91
m_inner_v (kg)	183111.164	453458.949	813922.661
m_outer_l (kg)	11293298.37	7058311.481	1411662.296
m_inner_l (kg)	720927.425	450579.641	90115.928

*Appendix A.4: Thermal Capacitance on the different parts of the wall*

<b>Description</b>	<b>Definition</b>	<b>80% filling level</b>	<b>50% filling level</b>	<b>10% filling level</b>	<b>Unit</b>
<b>Thermal mass of outer vertical wall in contact with the vapor space</b>	$C_1 = m_{o,v} * C_{p,v,o}$	2868428.835	7103415.724	12750064.91	kJ/K
<b>Thermal mass of inner vertical wall in contact with the vapor space</b>	$C_3 = m_{i,v} * C_{p,v,i}$	6335.646	15689.679	28161.724	kJ/K
<b>Thermal mass of outer vertical wall in contact with the liquid space</b>	$C_2 = m_{o,l} * C_{p,l,o}$	11293298.37	7058311.481	1411662.296	kJ/K
<b>Thermal mass of inner vertical wall in contact with the liquid space</b>	$C_4 = m_{i,l} * C_{p,l,i}$	2523245.987	1577028.742	315405.748	kJ/K

## References

- [1]. *Depleting Earth's resources* | MSUToday | Michigan State University. (n.d.). Retrieved January 21, 2021, from <https://msutoday.msu.edu/news/2018/depleting-earths-resources/>
- [2]. Brown, N. 2019 D., & Correspondent, E. (2019, November 1). *Hydrocarbons Expected to Remain the World's Primary Energy Source*. AAPG EXPLORER. <https://explorer.aapg.org/story/articleid/54995/hydrocarbons-expected-to-remain-the-worlds-primary-energy-source>
- [3]. *The future of hydrocarbons as a global energy source* | Ditchley Foundation. (n.d.). Retrieved January 21, 2021, from <https://www.ditchley.com/past-events/past-programme/2010-2019/2011/hydrocarbons>
- [4]. *The Paris Agreement* | UNFCCC. (n.d.). Retrieved March 8, 2021, from <https://unfccc.int/process-and-meetings/the-paris-agreement/the-paris-agreement>
- [5]. *Fossil fuels, explained*. (2019, April 2). Environment. <https://www.nationalgeographic.com/environment/article/fossil-fuels>
- [6]. *Transportation Fuel Market—Industry Analysis, Share, Size, Forecast 2022*. (n.d.). Retrieved March 8, 2021, from <https://www.transparencymarketresearch.com/transportation-fuel-market.html>
- [7]. Green, V. V., Kate Abnett, Matthew. (2020, August 18). *Explainer: Cleaner but not clean - Why scientists say natural gas won't avert climate disaster*. Reuters. <https://www.reuters.com/article/us-usa-gas-climatebox-explainer-idUSKCN25E1DR>
- [8]. » *Natural Gas in the Transportation Sector* NaturalGas.org. (n.d.). Retrieved January 22, 2021, from <http://naturalgas.org/overview/uses-transportation/>
- [9]. Qingfang, K., Shaocheng, C., Longshan, Z., & Miao, Y. (n.d.). *THE TRENDS OF LNG/CNG APPLICATION IN THE TRANSPORTATION INDUSTRY IN CHINA*. 27.
- [10]. Aursand, E., & Hammer, M. (2018). Predicting triggering and consequence of delayed LNG RPT. *Journal of Loss Prevention in the Process Industries*, 55, 124–133. <https://doi.org/10.1016/j.jlp.2018.06.001>
- [11]. *Liquefied natural gas—U.S. Energy Information Administration (EIA)*. (n.d.). Retrieved January 22, 2021, from <https://www.eia.gov/energyexplained/natural-gas/liquefied-natural-gas.php>
- [12]. *Benefits of LNG – Benefits Of*. (n.d.). Retrieved January 22, 2021, from <http://benefitof.net/benefits-of-lng/>
- [13]. *GasLog: LNG Demand Grew 9% in 2018*. (2019, February 14). MarineLink. <https://www.marinelink.com/news/gaslog-lng-demand-grew-462927>
- [14]. *Perlite Insulated Double Shell Vertical Tank & Horizontal Tank*. (n.d.). TOYO KANETSU K.K. Retrieved January 22, 2021, from [https://www.toyokanetsu.co.jp/global/product/plant/small\\_scale\\_lng.html](https://www.toyokanetsu.co.jp/global/product/plant/small_scale_lng.html)
- [15]. Gakuo, J. W. (2020, July 14). 11 LNG Terminals You Should Know in 2020 & Upcoming LNG Projects. *Oil and Gas Industry*. <https://www.upstreamawards.com/lng-terminals/>

- [16]. Khan, M. (2018). Comparative Well-to-Tank energy use and greenhouse gas assessment of natural gas as a transportation fuel in Pakistan. *Energy for Sustainable Development*, 43, 38–59. <https://doi.org/10.1016/j.esd.2017.12.004>
- [17]. Corporation, I. H. I. (n.d.). *LNG Receiving Terminal, Storage Tank / Resources, Energy and Environment / Products / IHI Corporation*. IHI Corporation. Retrieved January 22, 2021, from [https://www.ihico.jp/en/products/resources\\_energy\\_environment/lng\\_cryogenic\\_strage/index.html](https://www.ihico.jp/en/products/resources_energy_environment/lng_cryogenic_strage/index.html)
- [18]. Lun, H., Filippone, F., Roger, D. C., & Poser, M. (n.d.). *DESIGN AND CONSTRUCTION ASPECTS OF POST-TENSIONED LNG STORAGE TANKS IN EUROPE AND AUSTRALASIA*. 6.
- [19]. *LNG global storage tank capacity by country 2020*. (n.d.). Statista. Retrieved January 22, 2021, from <https://www.statista.com/statistics/723079/lng-global-storage-tank-capacity-by-country/>
- [20]. Thierçault, J. (n.d.). *CRYOGENIC ABOVE GROUND STORAGE TANKS: FULL CONTAINMENT AND MEMBRANE COMPARISON OF TECHNOLOGIES*. 8.
- [21]. Chamberlain, G. (2006). Management of large LNG hazards. *International Gas Union World Gas Conference Papers*, 5.
- [22]. Jeon, G.-M., Park, J.-C., & Choi, S. (2021). Multiphase-thermal simulation on BOG/BOR estimation due to phase change in cryogenic liquid storage tanks. *Applied Thermal Engineering*, 184, 116264. <https://doi.org/10.1016/j.applthermaleng.2020.116264>
- [23]. Hassanvand, A., Hashemabadi, S. H., & Bayat, M. (2010). Evaluation of gasoline evaporation during the tank splash loading by CFD techniques. *International Communications in Heat and Mass Transfer*, 37(7), 907–913. <https://doi.org/10.1016/j.icheatmasstransfer.2010.05.011>
- [24]. Lee, J. H., Kim, Y. J., & Hwang, S. (2015). Computational study of LNG evaporation and heat diffusion through a LNG cargo tank membrane. *Ocean Engineering*, 106, 77–86. <https://doi.org/10.1016/j.oceaneng.2015.06.045>
- [25]. Fu, J., Sunden, B., Chen, X., & Huang, Y. (2015). Influence of phase change on self-pressurization in cryogenic tanks under microgravity. *Applied Thermal Engineering*, 87, 225–233. <https://doi.org/10.1016/j.applthermaleng.2015.05.020>
- [26]. Zakaria, M. S., Osman, K., Saadun, M. N. A., Manaf, M. Z. A., & Mohd Hanafi, M. H. (2013). *Computational Simulation of Boil-Off Gas Formation inside Liquefied Natural Gas Tank Using Evaporation Model in ANSYS Fluent*. Applied Mechanics and Materials; Trans Tech Publications Ltd. <https://doi.org/10.4028/www.scientific.net/AMM.393.839>
- [27]. Ahammad, M., Liu, Y., Olewski, T., Véhot, L. N., & Mannan, M. S. (2016). Application of Computational Fluid Dynamics in Simulating Film Boiling of Cryogenics. *Industrial & Engineering Chemistry Research*, 55(27), 7548–7557. <https://doi.org/10.1021/acs.iecr.6b01013>

- [28]. Saleem, A., Farooq, S., Karimi, I. A., & Banerjee, R. (2018). A CFD simulation study of boiling mechanism and BOG generation in a full-scale LNG storage tank. *Computers & Chemical Engineering*, *115*, 112–120. <https://doi.org/10.1016/j.compchemeng.2018.04.003>
- [29]. Dobrota, D., Lalić, B., & Komar, I. (2013). Problem of Boil—Off in LNG Supply Chain. *Transactions on Maritime Science*, *02*, 91–100. <https://doi.org/10.7225/toms.v02.n02.001>
- [30]. 2019 World LNG Report. (n.d.). *IGU*. Retrieved January 23, 2021, from <https://igu.org/news/2019-world-lng-report/>
- [31]. Wang, X., Xu, Y., Wang, S., Xu, Q., & Ho, T. C. (2020). Comprehensive study on boil-off gas generation from LNG road tankers under simultaneous impacts of heat leakage and transportation vibration. *Fuel*, *275*, 117876. <https://doi.org/10.1016/j.fuel.2020.117876>
- [32]. Chen, Q.-S., Wegrzyn, J., & Prasad, V. (2004). Analysis of temperature and pressure changes in liquefied natural gas (LNG) cryogenic tanks. *Cryogenics*, *44*, 701–709. <https://doi.org/10.1016/j.cryogenics.2004.03.020>
- [33]. Migliore, C., Migliore, C., Tubilleja, C., & Vesovic, V. (2015). Weathering prediction model for stored liquefied natural gas (LNG). *Journal of Natural Gas Science and Engineering*. <https://doi.org/10.1016/J.JNGSE.2015.06.056>
- [34]. Yu, P., Yin, Y., Wei, Z., & Yue, Q. (2020). A prototype test of dynamic boil-off gas in liquefied natural gas tank containers. *Applied Thermal Engineering*, *180*, 115817. <https://doi.org/10.1016/j.applthermaleng.2020.115817>
- [35]. *Term*. (n.d.). Encyclopedia. Retrieved January 27, 2021, from <https://www.wartsila.com/encyclopedia/term>
- [36]. Arrhenius, K., Karlsson, A., Hakonen, A., Ohlson, L., Yaghooby, H., & Bükér, O. (2018). Variations of fuel composition during storage at Liquefied Natural Gas refuelling stations. *Journal of Natural Gas Science and Engineering*, *49*, 317–323. <https://doi.org/10.1016/j.jngse.2017.11.014>
- [37]. Huerta, F., & Vesovic, V. (2019). A realistic vapour phase heat transfer model for the weathering of LNG stored in large tanks. *Energy*, *174*, 280–291. <https://doi.org/10.1016/j.energy.2019.02.174>
- [38]. Shah, J. M., & Aarts, J. J. (1995). Effect of Weathering of LNG in Storage Tanks. In K. D. Timmerhaus (Ed.), *Advances in Cryogenic Engineering* (pp. 253–260). Springer US. [https://doi.org/10.1007/978-1-4613-9847-9\\_31](https://doi.org/10.1007/978-1-4613-9847-9_31)
- [39]. Adom, E., Islam, S., & Ji, X. (2010). *Modelling of Boil-Off Gas in LNG Tanks: A Case Study*. Undefined. [/paper/Modelling-of-Boil-Off-Gas-in-LNG-Tanks%3A-A-Case-Adom-Islam/700c138e68d114d6b593c4c7f2f2af8fd791ede1](https://doi.org/10.1007/978-1-4613-9847-9_31)
- [40]. Pellegrini, L. A., Molioli, S., Brignoli, F., & Bellini, C. (2014). LNG Technology: The Weathering in Above-Ground Storage Tanks. *Industrial & Engineering Chemistry Research*, *53*(10), 3931–3937. <https://doi.org/10.1021/ie404128d>
- [41]. Migliore, C., Salehi, A., & Vesovic, V. (2017). A non-equilibrium approach to modelling the weathering of stored Liquefied Natural Gas (LNG). *Energy*, *124*, 684–692. <https://doi.org/10.1016/j.energy.2017.02.068>

- [42]. Effendy, S., Khan, M. S., Farooq, S., & Karimi, I. A. (2017). Dynamic modelling and optimization of an LNG storage tank in a regasification terminal with semi-analytical solutions for N<sub>2</sub>-free LNG. *Computers & Chemical Engineering*, 99, 40–50.  
<https://doi.org/10.1016/j.compchemeng.2017.01.012>
- [43]. Roh, S., & Son, G. (2012). Numerical study of natural convection in a liquefied natural gas tank. *Journal of Mechanical Science and Technology*, 26(10), 3133–3140.  
<https://doi.org/10.1007/s12206-012-0820-x>
- [44]. Wang, Z., Sharafian, A., & Mérida, W. (2020). Non-equilibrium thermodynamic model for liquefied natural gas storage tanks. *Energy*, 190, 116412.  
<https://doi.org/10.1016/j.energy.2019.116412>
- [45]. *Isothermal Properties*. (n.d.). National Institute of Standards and Technology. Retrieved January 31, 2021, from  
[https://webbook.nist.gov/cgi/fluid.cgi?ID=C74828&TUnit=K&PUnit=MPa&DUnit=mol%2Fl&HUnit=kJ%2Fmol&WUnit=m%2Fs&VisUnit=uPa\\*s&STUnit=N%2Fm&Type=IsoTherm&RefState=DEF&Action=Page](https://webbook.nist.gov/cgi/fluid.cgi?ID=C74828&TUnit=K&PUnit=MPa&DUnit=mol%2Fl&HUnit=kJ%2Fmol&WUnit=m%2Fs&VisUnit=uPa*s&STUnit=N%2Fm&Type=IsoTherm&RefState=DEF&Action=Page)
- [46]. Lemmon, E. W., Huber, M. L., & McLinden, M. O. (2007). *NIST Standard Reference Database 23: Reference Fluid Thermodynamic and Transport Properties-REFPROP, Version 8.0*. <https://www.nist.gov/publications/nist-standard-reference-database-23-reference-fluid-thermodynamic-and-transport-0>
- [47]. Beduz, C., & Scurlock, R. G. (1994). Evaporation Mechanisms and Instabilities in Cryogenic Liquids. In P. Kittel (Ed.), *Advances in Cryogenic Engineering* (pp. 1749–1757). Springer US. [https://doi.org/10.1007/978-1-4615-2522-6\\_214](https://doi.org/10.1007/978-1-4615-2522-6_214)
- [48]. A Pressure Iteration Scheme for Two-Phase Flow Modeling. (2013). In *Computational Methods for Two-Phase Flow and Particle Transport* (Vol. 1–0, pp. 61–82). WORLD SCIENTIFIC. [https://doi.org/10.1142/9789814460286\\_0004](https://doi.org/10.1142/9789814460286_0004)
- [49]. Scurlock, R. G. (2016). Surface Evaporation of Cryogenic Liquids, Including LNG and LPG. In R. G. Scurlock (Ed.), *Stratification, Rollover and Handling of LNG, LPG and Other Cryogenic Liquid Mixtures* (pp. 41–62). Springer International Publishing.  
[https://doi.org/10.1007/978-3-319-20696-7\\_4](https://doi.org/10.1007/978-3-319-20696-7_4)
- [50]. Wood, D. A., & Kulitsa, M. (2018). Weathering/Ageing of Liquefied Natural Gas Cargoes During Marine Transport and Processing on Floating Storage Units and FSRU. *Journal of Energy Resources Technology*, 140(102901). <https://doi.org/10.1115/1.4039981>
- [51]. Khan, M. S., Qyyum, M. A., Ali, W., Wazwaz, A., Ansari, K. B., & Lee, M. (2020). Energy Saving through Efficient BOG Prediction and Impact of Static Boil-off-Rate in Full Containment-Type LNG Storage Tank. *Energies*, 13(21), 5578.  
<https://doi.org/10.3390/en13215578>

- [52]. Bergman T.l., Lavine A.s., Dewitt D.p., Incropera F.p. -*Introduction To Heat Transfer-john Wiley & Sons (2011).pdf [jlk9j8k05045]*. (n.d.). Retrieved February 2, 2021, from <https://idoc.pub/download/bergman-tl-lavine-as-dewitt-dp-incropera-fp-introduction-to-heat-transfer-john-wiley-sons-2011pdf-jlk9j8k05045>
- [53]. *Economic evaluation of BOG management systems with LNG cold energy recovery in LNG import terminals considering quantitative assessment of equipment failures | Elsevier Enhanced Reader*. (n.d.). <https://doi.org/10.1016/j.applthermaleng.2018.08.029>
- [54]. *Methane—Thermophysical Properties*. (n.d.). Retrieved February 6, 2021, from [https://www.engineeringtoolbox.com/methane-d\\_1420.html](https://www.engineeringtoolbox.com/methane-d_1420.html)
- [55]. Churchill, S. W., & Chu, H. H. S. (1975). Correlating equations for laminar and turbulent free convection from a vertical plate. *International Journal of Heat and Mass Transfer*, 18(11), 1323–1329. [https://doi.org/10.1016/0017-9310\(75\)90243-4](https://doi.org/10.1016/0017-9310(75)90243-4)
- [56]. Thierçault, J. (n.d.). *CRYOGENIC ABOVE GROUND STORAGE TANKS: FULL CONTAINMENT AND MEMBRANE COMPARISON OF TECHNOLOGIES*. 8.